AN ABSTRACT OF THE THESIS OF

John McBain Hubbe for the degree of Master of Science in Atmospheric Sciences presented on June 12, 1984.

Title: The Suitability of Optical Particle Counters For Covariance Estimates of the Dry Deposition Velocity of Particulate Aerosols

Abstract approved: Redacted for Privacy

Paul C. Katen

Experimental work at the 1982 Dry Deposition Intercomparison Experiment (DDIEx) involved the use of optical particle counters for covariance estimates of dry deposition velocities of accumulation mode aerosols. Meteorological and particle flux observations are presented. Deposition velocity estimates exhibit scatter about zero. A formulation of the standard error of the deposition velocity estimator is derived and examined. Using this formulation, the observed deposition velocities are shown to be marginally significant. Using a case study, the correlation coefficient is examined and presented as an important statistic to the work. Humidity effects on the measurements are briefly examined. Recommendations are made for improvements in the instrumentation.

The Suitability of Optical Particle Counters For Covariance Estimates of the Dry Deposition Velocity of Particulate Aerosols

by

John McBain Hubbe

A THESIS

submitted to

Oregon State University

in partial fulfillment of
the requirements for the
degree of

Master of Science

Completed June 12, 1984

Commencement June 1985

APPROVED:

Redacted for Privacy

Research Associate of Atmospheric Sciences in Charge of Major

Redacted for Privacy

Chairman of Department of Atmospheric Sciences

Redacted for Privacy

Dean of Graduate School

Date thesis is presented June 12, 1984

Typed by Diana Reynolds for John M. Hubbe

ACKNOWLEDGEMENTS

It is a priviledge to acknowledge the involvement of a number of people in this work. Their contributions have not only made it possible but made it an exciting learning experience.

Dr. Paul C. Katen has been my major professor in this degree and was the principal investigator in this work. From him I have received a foundation in field work and instrumentation. Through months of laborious and exhaustive analysis his perspective and perserverance kept me on track. I will always be grateful for his generosity. My minor professor was Dr. Richard W. Boubel who has also been very generous to me, both through his insight and experience shown during course work and in the professional realm. Dr. Larry J. Mahrt and Michael Schuyler also served on my committee and both contributed significantly to the thesis in content and form.

I will never forget my first opportunity in airborne field work and am grateful to Mike Wolf for providing it and for reviewing my final draft. I am grateful to Paul Stockton for his creativity and diligence in fabricating our instrumentation and for his friendship. It was a pleasure and a priviledge to work along side Dr. Marvin Wesely and David Cook at DDIEx. Of the entire faculty in the OSU Department of Atmospheric Sciences who have been helpful during my years here, Drs. Esbensen and Deardorff took particular interest in my work and the tools needed to perform it.

I am thankful to Robert Heald and Naomi Zielinski for helping guide drafts through a maze of electronic channels and to Diana Reynolds for all final word processing.

Of course this would be incomplete without recognition of the unending support of my wife Mary Lu. She is an inspiration.

This work was supported by the Environmental Protection Agency under grant number R80-7902-01-0.

TABLE OF CONTENTS

LIST OF FIGURES

LIST OF FIGURES (Continued)

LIST OF FIGURES (Continued)

LIST OF TABLES

THE SUITABILITY OF OPTICAL PARTICLE COUNTERS FOR COVARIANCE ESTIMATES OF THE DRY DEPOSITION VELOCITY OF PARTICULATE AEROSOLS

1. INTRODUCTION

In modeling meteorological transport of pollutants, one of the required parameterizations is the pollutant removal rate at the atmosphere's lower boundary due to dry processes, called the dry deposition. The vertical flux (F) of pollutants at the lowest level of the model, is often parameterized in terms of a deposition velocity (v_d) multiplied by the pollutant concentration (x) at that level (Wesely et al., 1977):

$$F = - v_d(z)\ x(z) \qquad (1.1)$$

where v_d is positive downward.

This thesis is concerned with the deposition velocity to a grass covered surface of particles in the accumulation mode and the micrometeorological methods used to measure this quantity. The accumulation mode in the aerosol size spectrum is generally considered to include particle diameters between 0.1 and 1.0 μm.

Theoretical predictions of particle deposition velocity are calculated in terms of particle variables, diameter and density, and micrometeorological parameters, aerodynamic surface roughness, friction velocity and height above the surface (Sehmel, 1980). As an example of these theoretical calculations, predicted deposition velocities are

illustrated in Figure 1.1 over a range of surface conditions and particle densities. While this figure represents a stable atmosphere, the curves are qualitatively similar to the neutral or unstable cases which are considered herein. When v_d is evaluated as a function of particle size, it has a minimum over the range 0.1 to 1.0 μm under typical conditions. This minimum represents equivalent contributions of Brownian diffusion velocity and Stokes (gravitational) fall speed. The magnitudes of the two processes decrease and increase respectively with particle size. An additive contribution to the deposition velocity for particles of diameters greater than 1 micron, (Sehmel 1980, p 1003) is the eddy diffusivity.

Methods for measuring vertical flux, from which deposition velocity is estimated, can be categorized primarily as collection methods and micrometeorological methods. There is a wide variety of collectors including bucket collectors, artificial surfaces such as sticky papers, filter papers, glass dishes and also selected natural surfaces such as tree leaves, grass, soil or snow. Micrometeorological methods include estimates based on vertical profiles of average concentrations, covariance of vertical wind and concentration ("covariance", "eddy flux" or "eddy correlation" method) and the eddy accumulation method in which one of two filters is aspirated in proportion to the magnitude of the vertical wind (one for up-drafts; the other for down-drafts.) These methods, and individual experiments using a given method, have produced widely varying estimates of the deposition velocity for a given surface.

The covariance method estimates the deposition velocity from micrometeorological measurements made at a single level in the surface

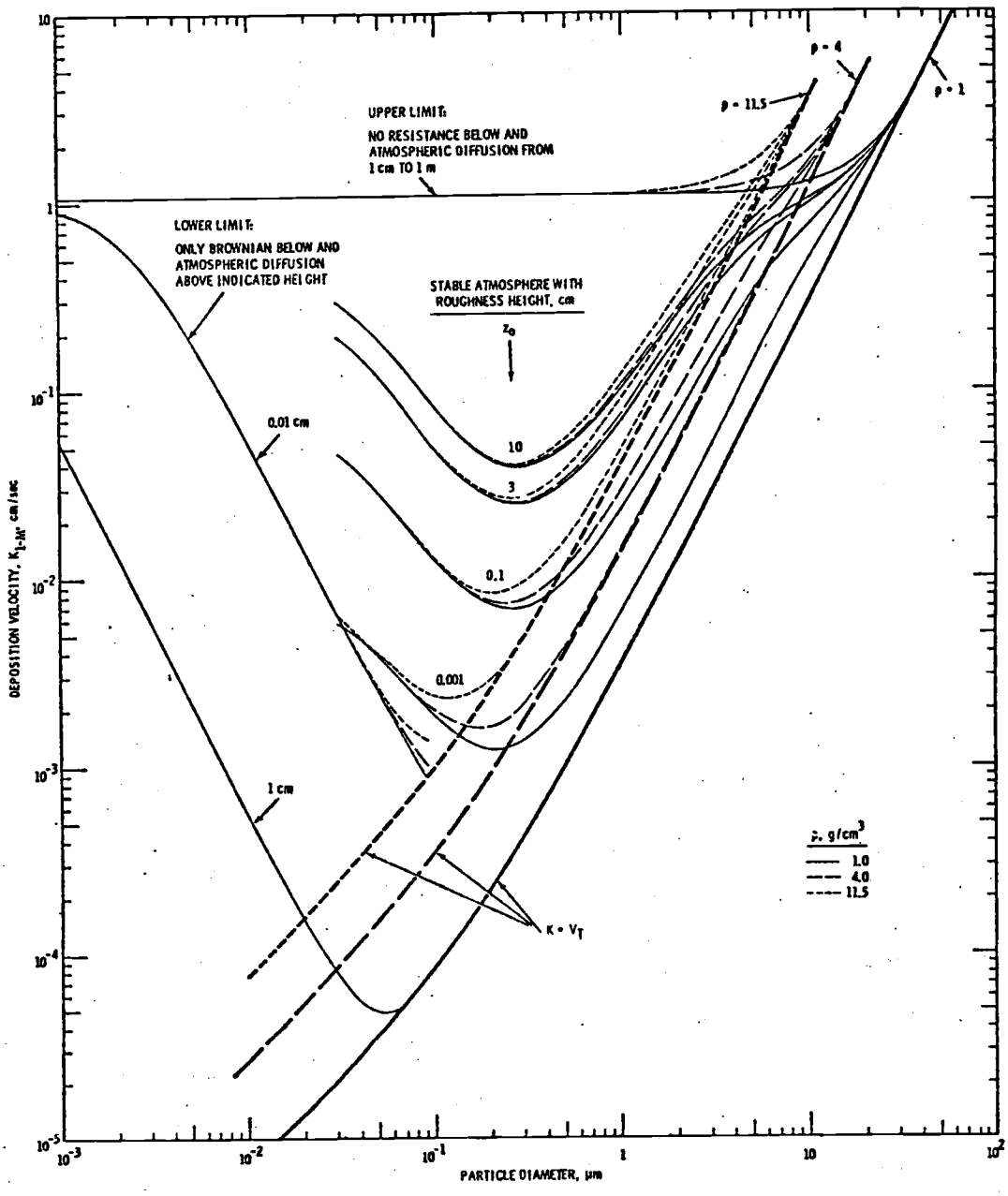

Figure 1.1
Predicted deposition velocities at 1 m for u_*=30 cm s^{-1} and particle densities of 1, 4, and 11.5 g cm^{-3} (from Sehmel, 1980).

layer; usually from a tower or airborne platform. The estimated deposition velocity, v_d, is calculated according to

$$v_d = - \frac{\overline{w'x'}}{\bar{x}} \qquad (1.2)$$

in which $\overline{w'x'}$ is the sample covariance of the vertical wind (w) and the concentration (x) and $\bar{x}$ is the sample mean of x. In this notation, w' and x' are deviations from the sample means $\bar{w}$ and $\bar{x}$ respectively, such that in theory $\overline{w'}=0$ and $\overline{x'}=0$.

The deposition velocity is intended to account for pollutant removal by the earth's surface. The basis for inference of a surface process from measurements made remote from the surface is the validity of the assumption that the vertical divergence of the flux, in the layer between the sensor and the surface, is small compared to the flux itself. Conditions which validate this assumption are well documented for fluxes of momentum and heat (Kaimal et al., 1972) and for fluxes of water vapor and other traces gases as well (Hicks & Wesely, 1981; Wesely et al., 1982) and this assumption is usually made in the lowest portion of the boundary layer, known as the surface layer. With regard to fluxes of particulate matter, the validity of the assumption (or rather the satisfaction of experimental constraints which validate the assumption) is being discussed in current literature (Slinn, 1983; Hicks et al., 1980) and will continue to be examined in on-going experimental work.

In many recent works (e.g. Wesely et al., 1983; Wesely et al., 1981; Smith & Jones, 1979; Webb et al., 1980; Brook, 1978; Neumann &

den Hartog, 1984) an additive correction to this estimate has been applied as

$$v_d = - \frac{\overline{w'x'}}{\overline{x}} - \overline{w} \qquad (1.3)$$

to account for a non-zero mean vertical velocity resulting from density fluctuations associated with Reynolds flux of heat and water vapor. All authors do not agree that this correction must be made (Brook, 1978) but discussion of that issue is beyond the scope of this work (however, valuable background may be found in Waldmann & Schmitt, 1966 and Goldsmith & May, 1966.) For reasons which are explained in section 5, this correction is not made in the present data analysis.

There remains considerable uncertainty even as to the true order of magnitude of the dry deposition velocity over grass of particulate aerosols in the accumulation mode (Sehmel, 1980; Hosker & Lindberg, 1982) Theoretical predictions indicate that values should be on the order of 0.01 cm/s (Slinn, 1983). Wind tunnel experiments also indicate that V_d is on this order of magnitude (Sehmel, 1973). Several field studies, however, suggest that v_d takes on values greater than 0.1 cm/s (Wesely et al., 1977; Wesely & Hicks, 1979; Sievering, 1982)

Early field work was performed using aerosol particle chargers (Wesely et al., 1977) to measure particle concentration. Subsequent work used integrating nephelometers (Slinn et al., 1979) and most recently, optical particle counters and aerosol spectrometers (both referred to here simply as OPCs, without dwelling on the distinction) have been used (Sievering, 1983; Katen & Hubbe, 1984; Neumann & den Hartog, 1984.) Most effort has been directed toward development and

use of OPCs primarily because of their good size resolution. The motivation has been to examine experimentally the functional dependence of deposition velocity on particle size.

The objective of this thesis is to present experimental evidence on the suitability of OPCs for use in the covariance method of estimating the dry deposition velocity of accumulation-mode particulate aerosols. The material presented to meet this objective is organized into the following sections: (2) a description of the field experiment which was based on the covariance method and a summary of the analytical methods used; (3) a presentation of the experimental observations and deposition velocity estimates; (4) an analysis of the sources of uncertainty in the estimates; (5) interpretation of the results, including case studies; (6) recomendations for improvements and variations in the sensors and experimental method.

2. EXPERIMENTAL PROCEDURE

2.1 Instrumentation

Based on a recent critique of methods (Hicks et al., 1980), accurate surface layer flux estimates may be achieved if the following conditions are met: 1) the frequency response of the sensors is sufficient (sensors are typically sampled at 10 Hz); 2) the sensors are operated at a height which is less than 0.5% of the uniform upwind fetch; and 3) "the sum of exponential response time and delay time of each sensor used should be less than [the platform] height divided by mean wind speed." Limited inadequacies in sensor response, which result in attenuation at high frequencies of the measured turbulent spectrum, may be corrected during data processing (Hicks, 1972).

The micrometeorological sensors used in this experiment were provided by teams from Oregon State University (OSU) and Argonne National Laboratory (ANL). Vertical wind was measured with a Gill helical propellor anemometer manufactured by R.M. Young & Co. Horizontal wind was measured with the ANL fast response "micro-cup" anemometer (Frenzen, 1967). Temperature was measured with a micro-bead thermistor (Hicks, 1970). Water vapor pressure was measured with a Lyman-alpha sensor.

The particle concentration sensors, two OPCs, are operated and maintained by the OSU team. One is a Particle Measurement Systems Active Scattering Aerosol Spectrometer model 300-A (PMS ASAS-300A). It has 15 linearly spaced sub-ranges of 4 size ranges as listed in Table 2.1, the lower detection limit being 0.15 μm. The other sensor is a

Table 2.1
Optical Partical Counter Size Ranges

ASAS-300A (15 channels):

Size Range Code	Size Range (μm)	Channel Width (μm)
0	.600-3.000	.160
1	.400-1.000	.040
2	.230-.605	.025
3	.150-.300	.010

Royco (10 channels):

Size Range (μm)	Approximate Channel Width (μm)
.30-2.5	0.2

Royco model 225, which in combination with a pulse height analyzer, has 10 subrange counting channels over the size range 0.3 to 2.5 μm indicated in Table 2.1.

For the purposes of faster sensor response and signal processing compatibility with the other sensors which produce analog voltages, interfaces were built for the two OPCs which generate analog voltages proportional to count rate. Each interface generates two signals to provide two switch selectable subsets of the counting channels of the respective OPC PHA. Thus, four particle concentration signals were monitored. The PMS and Royco signals are referred to as K1 and K2 and R1 and R2 respectively. Unless otherwise noted, these signals represent count rates or concentrations over size ranges as listed in Table 2.2. Also listed in Table 2.2 are mass median diameter (MMD) and mass weighted diameter (MWD) as calculated for each range.

One other device used in this field work was an analog covariance meter, a recent version of the type of instrument described by Hicks (1970). It is essentially an analog computer dedicated to the computation of the instantaneous eddy product ($w'x'$) and the integrated eddy product ($\int w'x'dt$), the latter being proportional to the covariance (the constant of proportionality is the inverse of the integration period.) It produces these two analog voltages for nine individual channels. The device also provides a bar-graph display, viewable on an oscilloscope, of input signals, (both before and after mean removal); of instantaneous products; and of integrated products. This feature was extremely valuable in the field, both for optimizing signal gains and for detecting trouble in sensor operation or signal transmission.

Table 2.2
Particle Size Ranges Covered by Particle Counter Signals

Instrument	Signal Code	Size Range (μm)	MMD (μm)	MWD (μm)
ASAS-300A	K1	0.15-0.21	0.18	0.17
	K2	0.21-0.30	0.25	0.24
Royco	R1	0.30-1.50	0.85	0.50
	R2	1.50-2.50	1.80	1.60

The data acquisition system consisted of a Hewlett-Packard 9825A desktop calculator with an HP 3495A scanner and a HP 3437A system voltmeter. Digital data was stored on a Dylon 9 track tape system.

2.2 Field Work

The Dry Deposition Intercomparison Experiment (DDIEx), during which the reported research was conducted, took place during June 1982 at the University of Illinois Montecello Road Field Site Southwest of Champaign, Illinois. The field work was performed in cooperation with Illinois State Water Survey (ISWS), coordinator of DDIEx, and with Argonne National Laboratory (ANL) through use of common micrometeorological sensors and field laboratory facilities. Towers were erected in an Array of Experiments (Figure 2.1) for sampling southerly wind conditions. Uniform fetch over grass was 200 m to the south and up to 400 m to the southeast and southwest. In addition to its proximity to ISWS, the site was chosen for the purpose of sampling well-mixed air pollutants originating in the St. Louis metropolitan area 230 km to the southwest. The ground cover was a well-established grass between 20 and 50 cm tall. Immediately beyond the perimeter of the grass field were fields of corn and soy beans.

Micrometerological sensors and the inlets of the OPCs were co-located at the six meter level on a boom extending upwind of a scaffold type tower (provided by ANL). All sensors or sensor inlets were within 40 cm of the vertical wind sensor and at least 150 cm from the scaffold. The ASAS-300A was operated in the "calibration insert" configuration which was aspirated by a positive displacement pump.

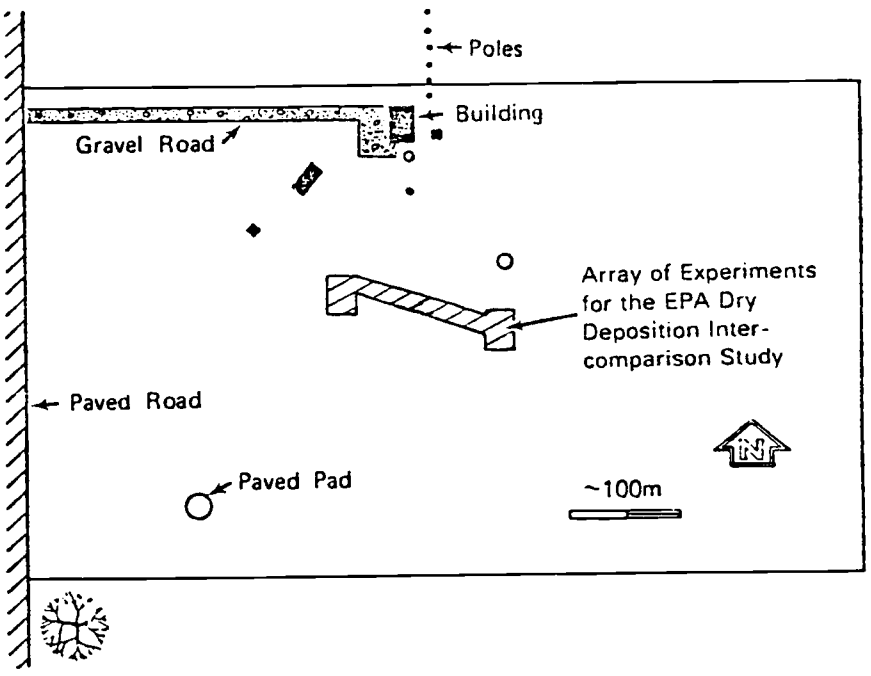

Figure 2.1: Map of Experimental Site.

Both OPCs used 0.44 cm ID inlet extensions made of aluminum to minimize electrostatic precipitation during transit.

Data acquisition was performed as follows. Sensor signals were first conditioned by a 10-channel bank of preamplifiers. At this stage, signals were low pass filtered (F_{CO}=5Hz) to prevent aliasing in sampled digital data. Then gains were applied to optimize the use of voltmeter precision. The vertical wind (w) signal and the four particle signals were digitized after this stage at a sample frequency of 10 Hz. These five along with temperature (T), wind speed (u) and vapor pressure (e) signals were input to the analog covariance meter with the w signal being common to all the resulting products. All of the covariance meter outputs (instantaneous and integrated eddy products) were digitized at a sample frequency of 1 Hz and selected integrator signals were monitored by a four-pen strip chart recorder in real time. Data blocks of 25 minutes centered on 15 and 45 minutes after the hour (CDT) were stored on digital magnetic tape. Primarily daytime conditions were monitored by the system due to the inadequacies of sensor response for resolving fluxes under highly stable conditions. In addition to this constraint, the system was not operated during rainy periods or when thunderstorms were imminent. A total of 461 blocks were digitized, a few of which represented altered instrument configuration for the purpose of quality control. Only about half of the total were suitable for flux estimates, as will be explained in a later section.

Half hour averages of temperature, relative humidity, pressure, precipitation, global radiation, and wind direction and speed were provided by ISWS.

2.3 Data Analysis

The majority of the data analysis associated with this experiment is comprised in four categories: algorithms for (1) digital estimates of fluxes and deposition velocities from raw digital data; (2) digital estimates of fluxes and deposition velocities from digitized covariance-meter data; (3) spectral analysis of raw digital data; and (4) data base management routines for screening, combining, summarizing and presenting the results of (1) through (3). Additional calculations were performed for the presentation of size distributions, for quality control and for the estimation of cross-covariance and auto-covariance as a function of lag.

The digital covariance algorithms had the following features. The vertical wind signal was lagged with respect to the particle count signals according to the delays resulting from sample transit time through the inlet extensions. For the purpose of removing the mean and low frequencies from the signals, a first order recursive high pass filter was used with half power at a frequency of 0.0016 Hz. This procedure of calculating Reynolds flux terms ultimately introduces additional terms in the turbulent kinetic energy equation but the enhanced stationarity of the signals and the economy of computing time were thought to outweigh biases which would be small if the spectral gap in the surface layer measurements is large. A case study of the spectra and cospectra of a block in which w, Kl, u, e, and T were digitized indicates that variances of the meteorological variables may be attenuated by between 4 and 35 percent and covariances by between 4 and 26 percent due to the chosen cutoff frequency. This case suggests

that although the particle signal variances were attenuated by less than 10%, their w-covariances may have been attenuated by a significant amount. However, alternate computation of all particle fluxes without the use of this filter shows no significant attenuation due to its use.

The analog covariance meter output signals, in addition to their use for real time monitoring of the system and conditions, were digitized for later processing. The best estimate derived from this instrument of flux during a 25 minute block was chosen to be the slope of a linear least squares fit to the time series of the integrated eddy product. As above, this estimate enhanced the stationarity of the series by minimizing the effect of small discontinuities in the flux process. Alternate analog derived estimates would be (1) the final value of the integrator time series and means of either (2) the instantaneous or (3) integrated eddy product time series (all of which were calculated for the purpose of quality control.)

Spectral analysis of the digitized data was performed for the purpose of documenting sensor response, noise characteristics and for examination of the frequency dependencies of the flux process. Standard Fast Fourier Transform (FFT) algorithms were used to calculate spectral and cospectral densities. Mean and trend removal was performed by the same first order recursive high pass filter as above. As indicated previously, all sensor signals were low pass filtered in the analog domain before being digitized in order to eliminate aliasing into the sampled frequency band. A cosine taper data window was applied in order to minimize leakage. The primary reason that this measure is important to this work is quality control

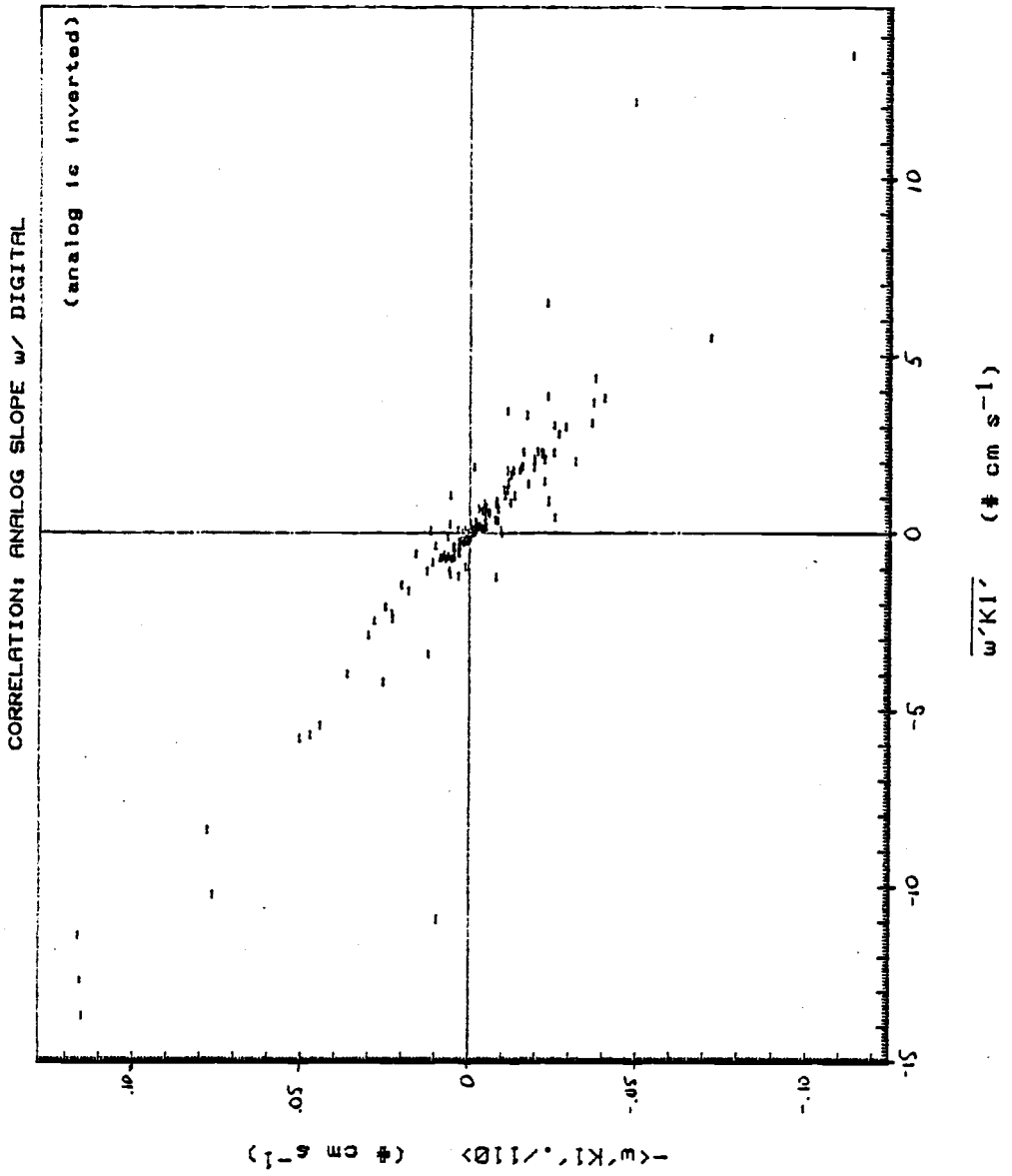

Figure 2.2:
Scattergram indicating correlation between analog and digital estimates of particle flux.

since the (population) turbulence spectra should be smooth. Harmonic contamination originating in sensors or in signal transmission or processing is more easily detected through the use of such a window since it inhibits leakage.

A 1024 point FFT was used; therefore spectra were calculated over two frequency bands for each 25 minute block: a high band in which spectral densities of 14 adjacent 1024 point sub-blocks were averaged; and a low band in which a single spectrum was calculated from a 1024 point block of 14 point averages. For graphic presentation, the 512 spectral densities in each band were smoothed by applying 25 equal logarithmic averaging intervals (as described by Kaimal, 1978.) Smoothed spectral densities were normalized and plotted as logarithmic spectra (nS(n)) against the logarithm of a non-dimensionalized frequency (f=nz/U in which n is the cyclic frequency, z is the instrumentation height and U is the sample mean wind speed.)

For the purpose of quality control, the described algorithms provide up to nine covariance estimates of vertical flux from which deposition velocity may be estimated. Comparison of the results of these analysis methods indicated first that all estimates were in reasonable agreement and also that the analog covariance meter performed very reliably. Figure 2.2, for example, indicates the degree of agreement between analog and digital estmates of covariance.

3. OBSERVATIONS

The observations made at the Dry Deposition Intercomparison Experiment will be divided into three categories. Meteorological observations will be used to define acceptable samples and also to characterize the micrometeorology of the site. Particle concentrations will be presented as background information for examination of fluxes. Finally, deposition velocity estimates will be presented.

As was indicated previously, the sensors were not operated during precipitation events or when the threat of electrical storms was high. A total of 461 blocks were digitized; of these, 272 had average 6 m wind directions in the sector between 110 and 250 degrees. This sector was chosen to eliminate any biases which may have resulted from wake effects of the row of towers. Except where noted, only data satisfying this wind direction criterion are presented herein.

The micrometeorology of the site and period may be characterized by surface-layer fluxes of momentum, sensible heat and water vapor. Figure 3.1a-c presents diurnal composites of the covariances representing these three quantities as calculated by the analog covariance meter. Each plotted point represents a 25 minute average of the pertinent quantity. Wind speeds are in units of cm/s; temperature is in degC; water vapor pressure is in mb; and hour of the day is in Central Daylight Time (CDT). In general, these plots verify the expected diurnal cycles in these fluxes and indicate the appropriate range of hours for estimating daytime fluxes (0800 to 1800). They also

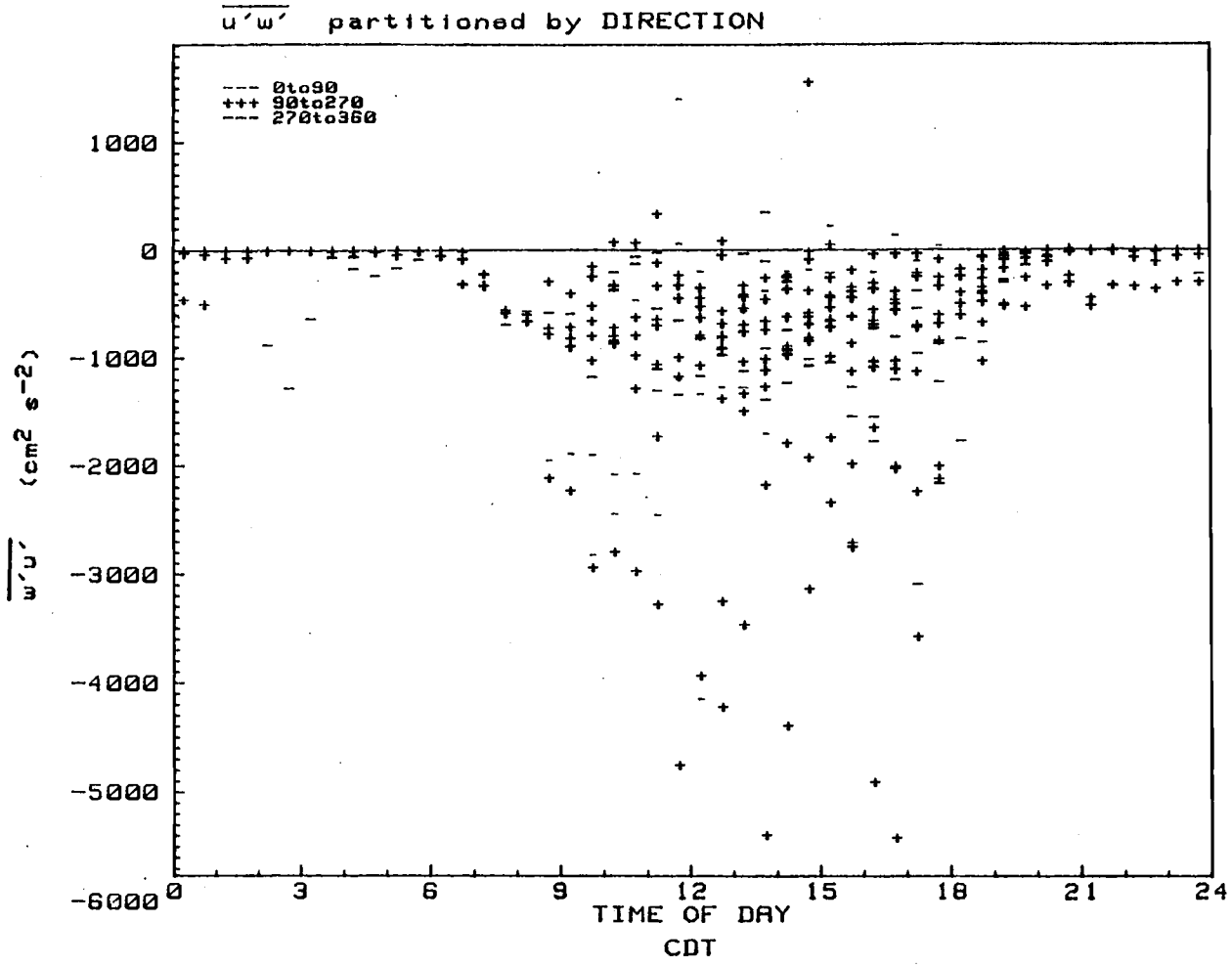

3.1a: Diurnal composite of $\overline{u'w'}$, partitioned by wind direction.

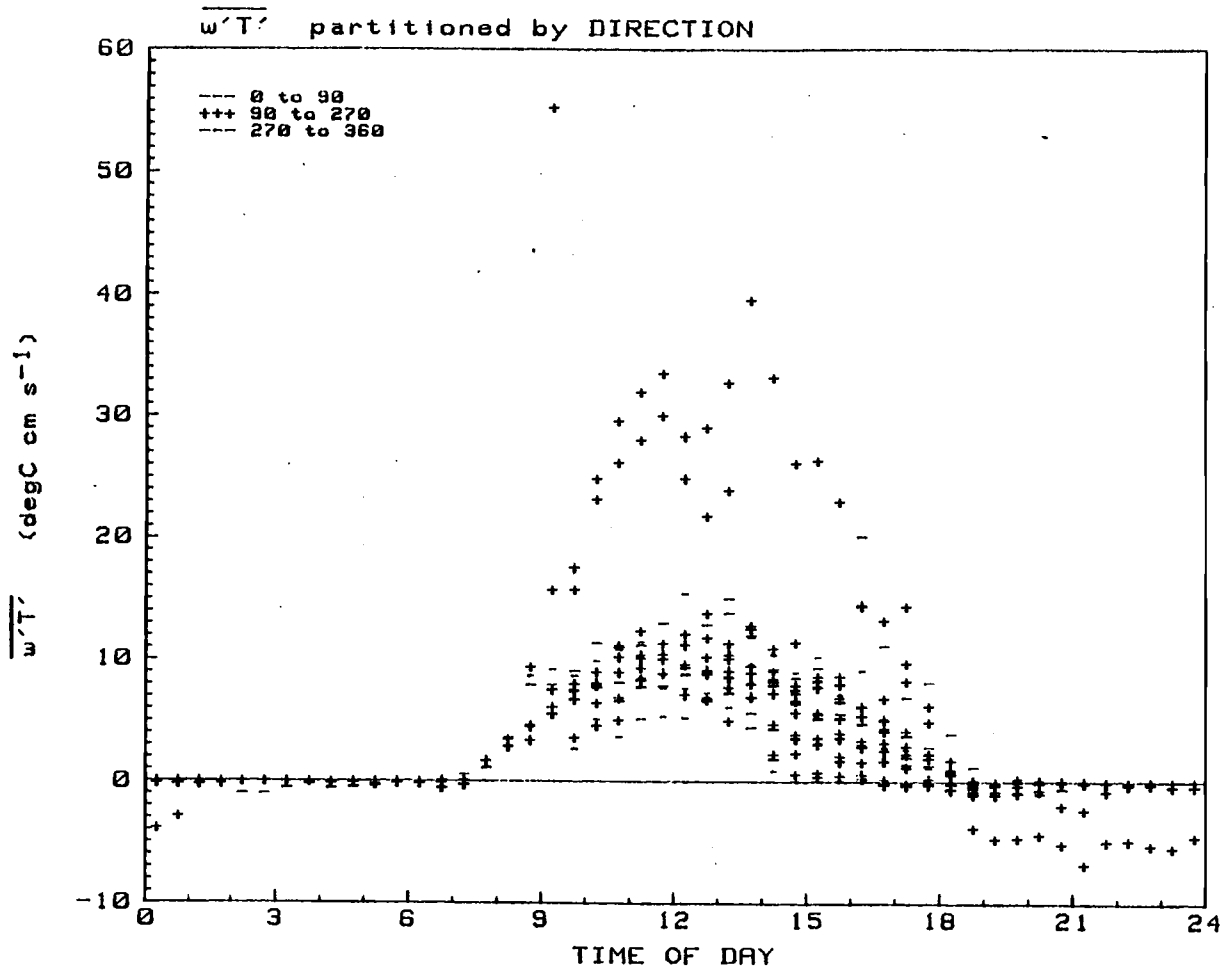

3.1b: Diurnal composite of $\overline{w'T'}$, partitioned by wind direction.

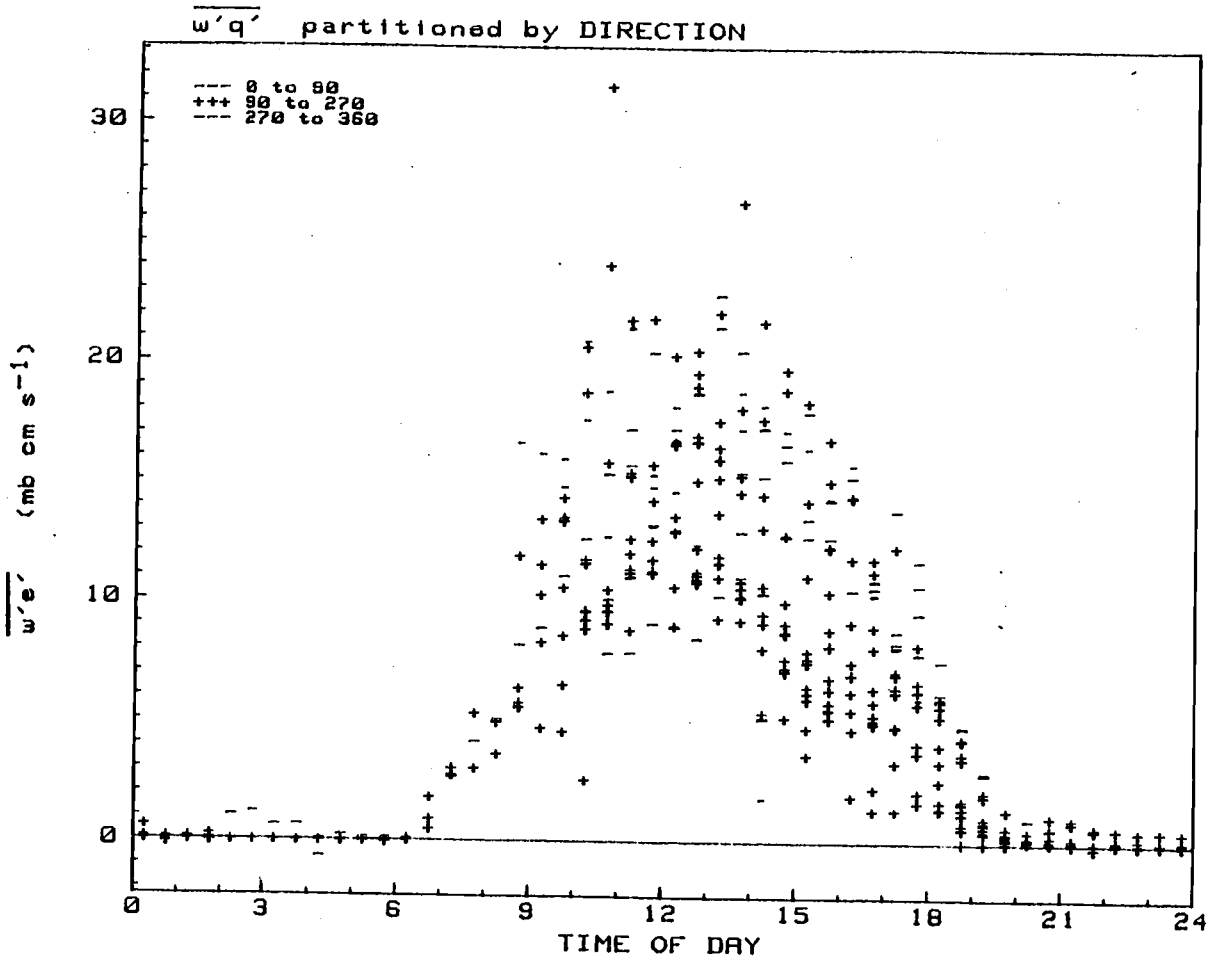

3.1c: Diurnal composite of $\overline{w'e'}$, partitioned by wind direction.

indicate that these fluxes varied, at midday, by at least a factor of two.

Specifically, $\overline{w'u'}$ varies between 0 and -1400 $cm^2 s^{-2}$ (a friction velocity, $0<u_*<37.4$ cm s^{-1}) for the bulk of the daytime blocks. The temperature covariance ($\overline{w'T'}$) varies between about 7 and 13 degC cm s^{-1} at midday with greater variability indicated during the afternoon than during morning hours (although this effect is exaggerated by the availability of fewer morning blocks.) This suggests more variability in insolation due to intermittant cloud cover in the afternoon and in turn implies convective activity; which in fact was commonly observed. The "vapor flux" ($\overline{w'e'}$) varies between approximately 10 and 22 mb cm/s at midday and also displays greater variabiliy during the afternoon than during the morning. This also is associated with frequent convective cloudiness. Note that vapor pressure (the quantity measured by the lyman-α sensor) is used here instead of specific humidity only for expedience. The small errors due to the non-conservation of vapor pressure are not of importance to this work.

A diurnal composite of relative humidity (RH) measured at the 6 m level by ISWS is given in Figure 3.2. Only those blocks corresponding to OSU operations are plotted. Finally, Figure 3.3 presents a small sample of the nondimensional stability parameter z/L, in which z is the instrumentation height and L is the Monin-Obukov length scale as calculated by ANL according to

$$L = \frac{\rho c_p u_*^3 \Theta}{kg(H+L_w E/14)} \qquad (3.1)$$

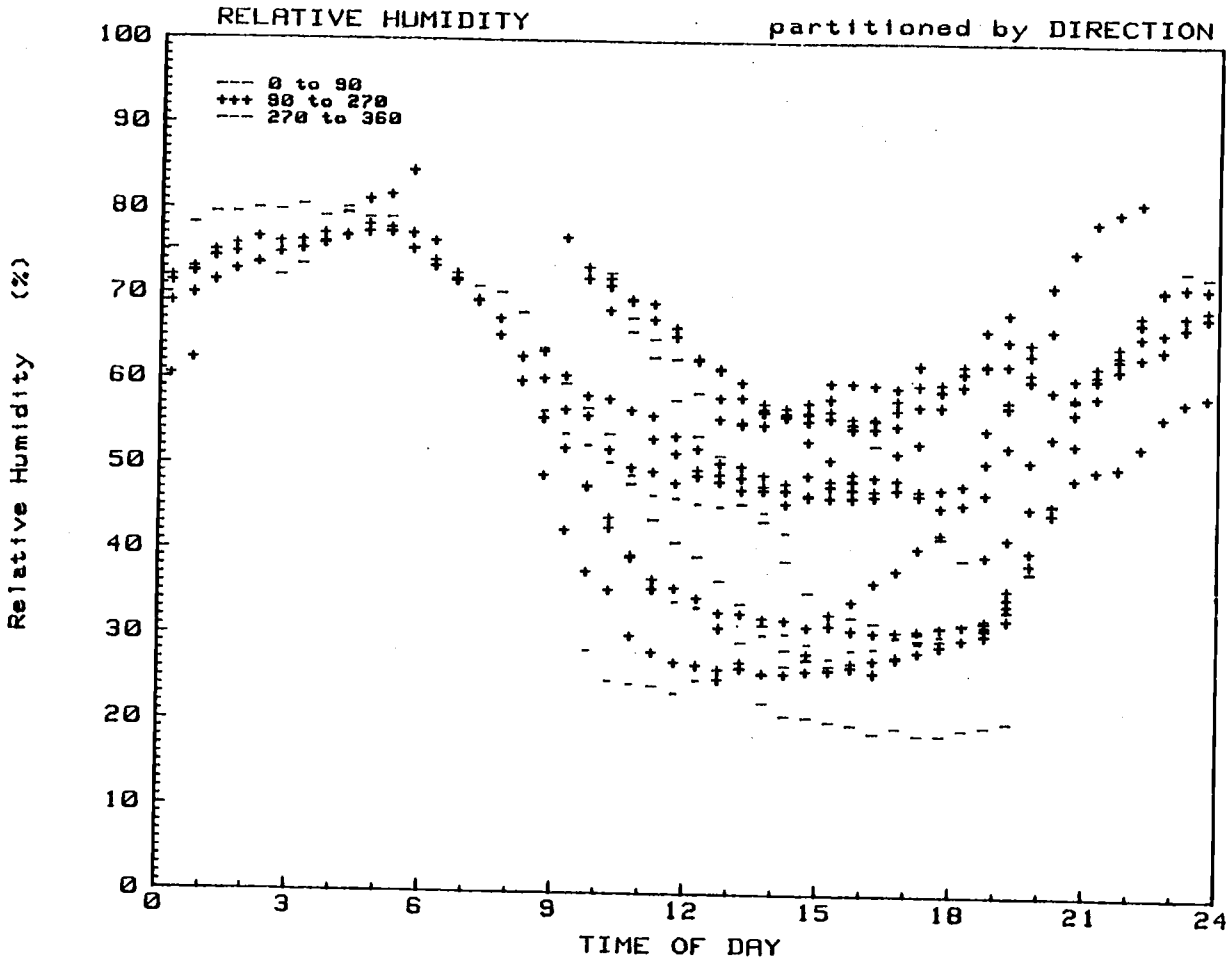

3.2: Diurnal composite of relative humidity, partitioned by wind direction.

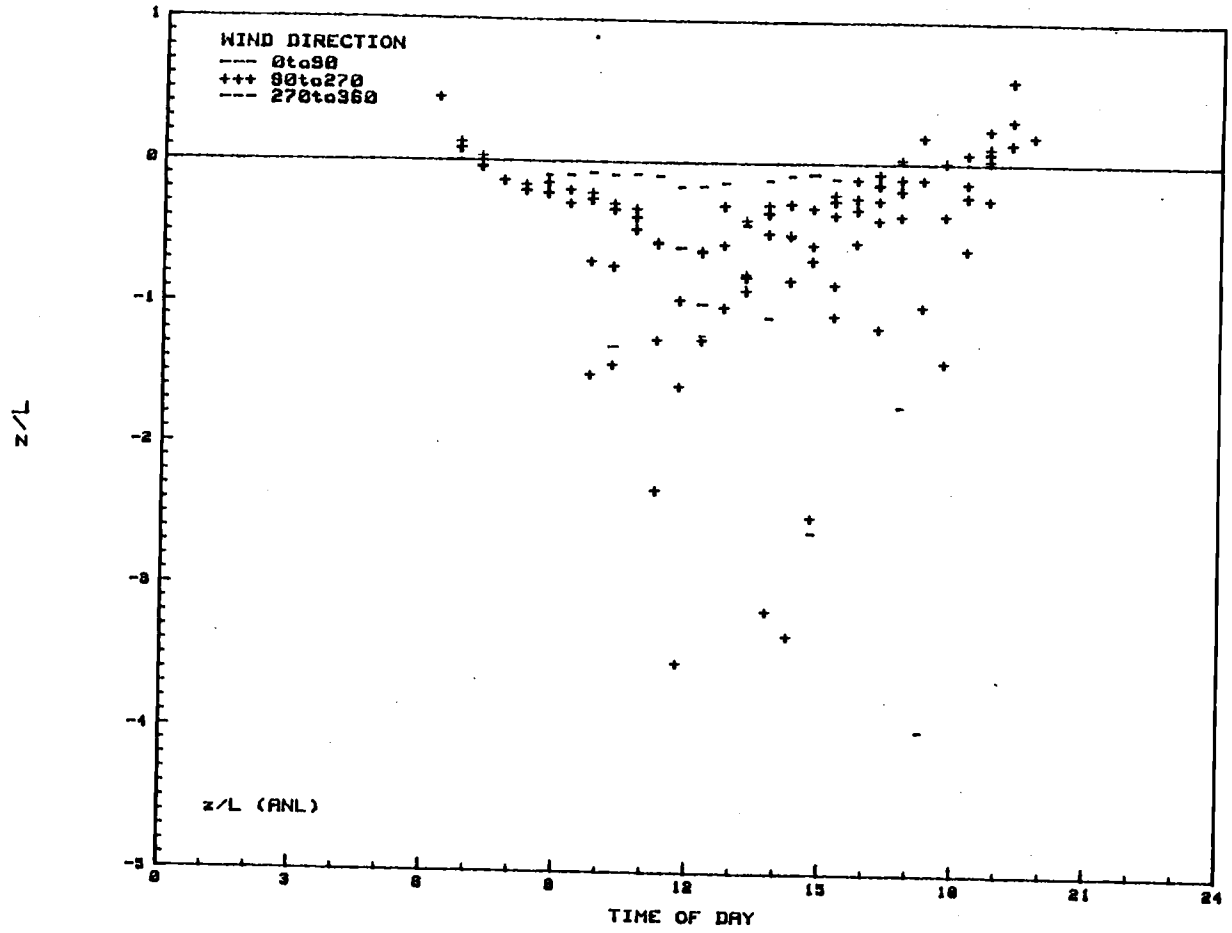

3.3: Diurnal composite of z/L, partitioned by wind direction.

in which ρ is air density, c_p is specific heat at constant pressure, θ is potential temperature, k is von Karman's constant, g is gravitational acceleration, H is sensible heat flux and L_wE is latent heat flux. The bulk of the unstable cases display a z/L magnitude smaller than two. Those outside this range occur with u_* less than 16 cm s^{-1}. Note also that ANL considered blocks to be useful only if $u_*>5$ cm s^{-1}.

Average particle count rates for the 25 minute blocks are presented in Figure 3.4a-d for the four particle count signals (K1, K2, R1, R2). The diurnal composite format will be useful for examining concentrations in Section 4. Count rates are plotted in units of #/0.2 s, and range between about 5 and 50 for the ASAS-300A sizes and up to several hundred for the Royco sizes with the distributions skewed to the lower values in all cases. Note that short sections of the individual time series can be seen through the composite and that these suggest a diurnal cycle.

Deposition velocity estimates based on analog calculations are presented (also in the diurnal composite format) in Figure 3.5a-d. The features of these data that should be noted are the ranges of the daytime values (+/-.3 cm s^{-1} for K1 and K2, -.6 to .4 cm s^{-1} for R1 and -.9 to .3 cm s^{-1} for R2) and the large degree of variability about zero particularly for the K1 and K2 size ranges. There is a strong diurnal cycle in the variance of these estimates, indicated by the strong damping during nighttime hours. The 50% to 70% relative humidity partition seems to account for a majority of the daytime negative deposition velocities except for K1. These features and their implications will be examined and discussed in subsequent sections.

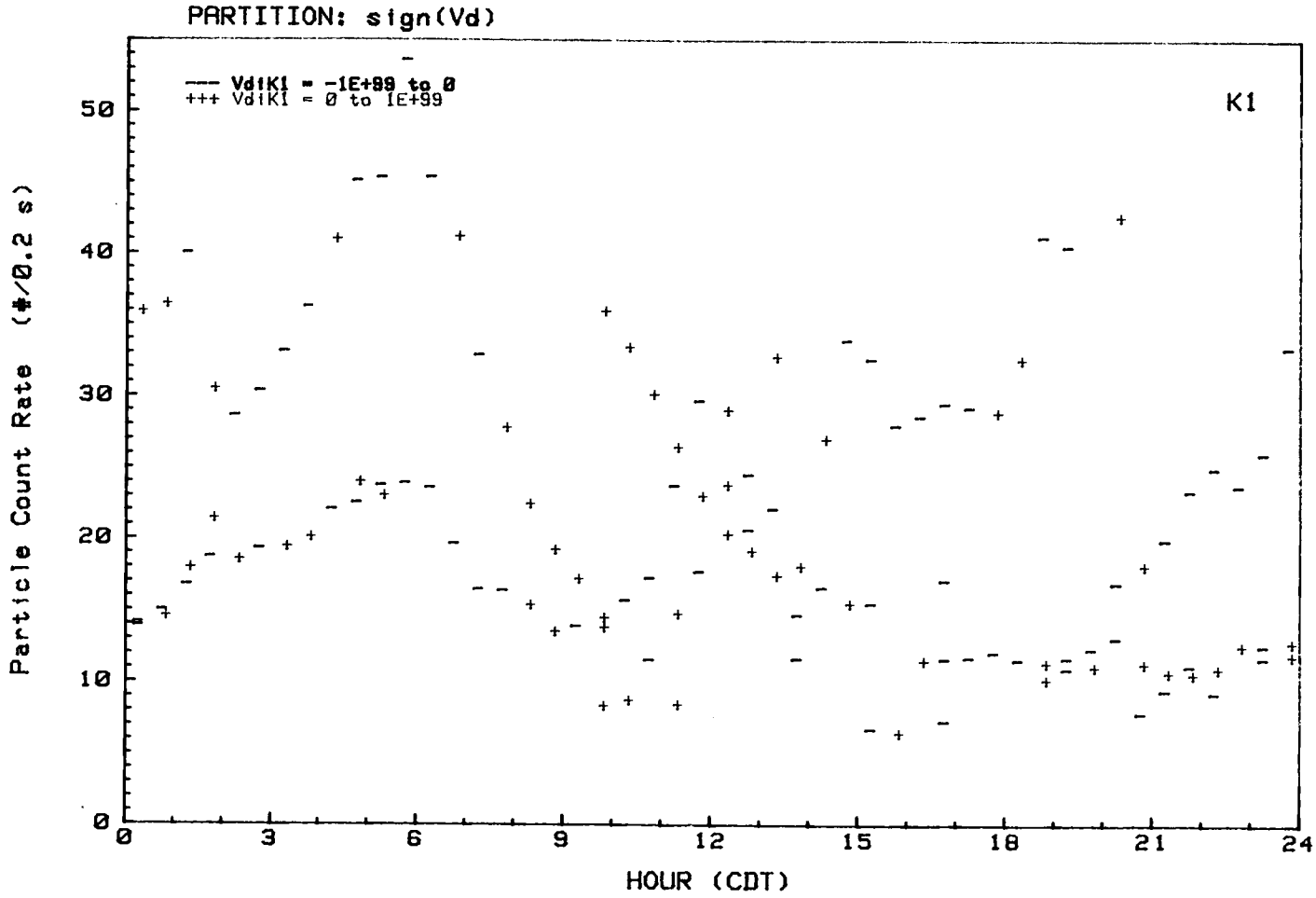

Figure 3.4a: Diurnal composite of particle count rate (K1), partitioned be sign of v_d.

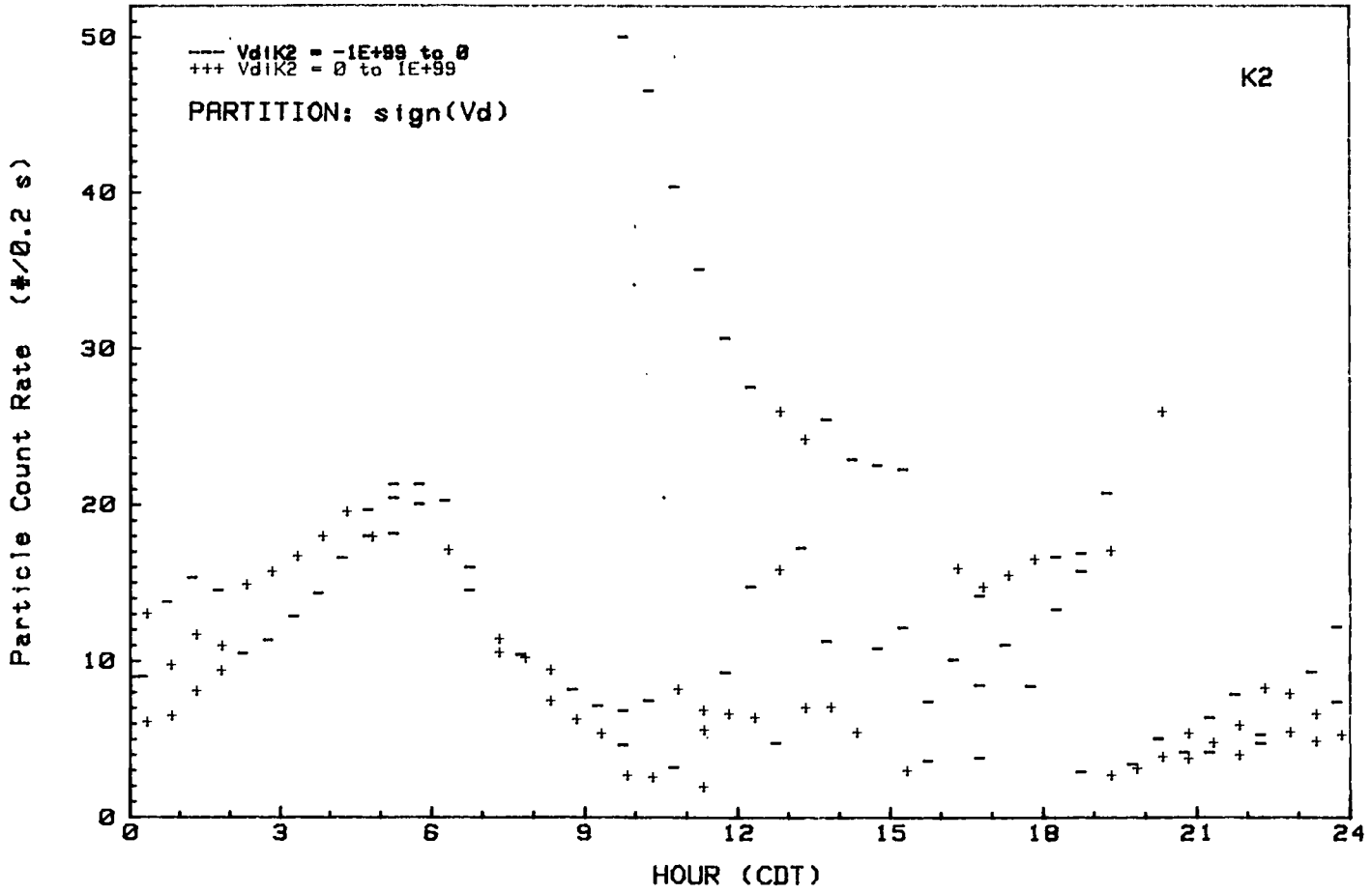

Figure 3.4b: Diurnal composite of particle count rate (K2), partitioned by sign of v_d.

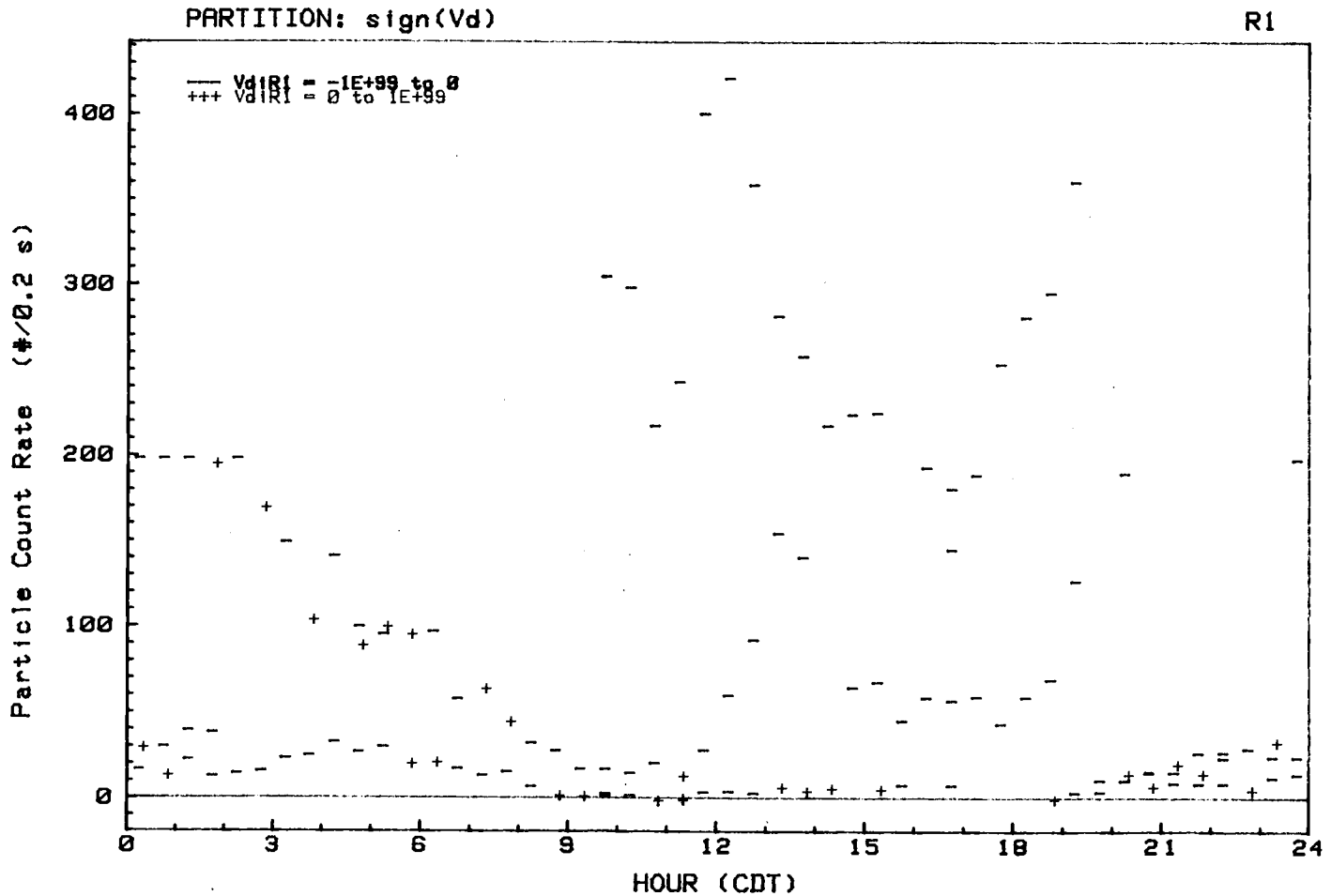

Figure 3.4c: diurnal composite of particle count rate (R1), partitioned be sign of v_d.

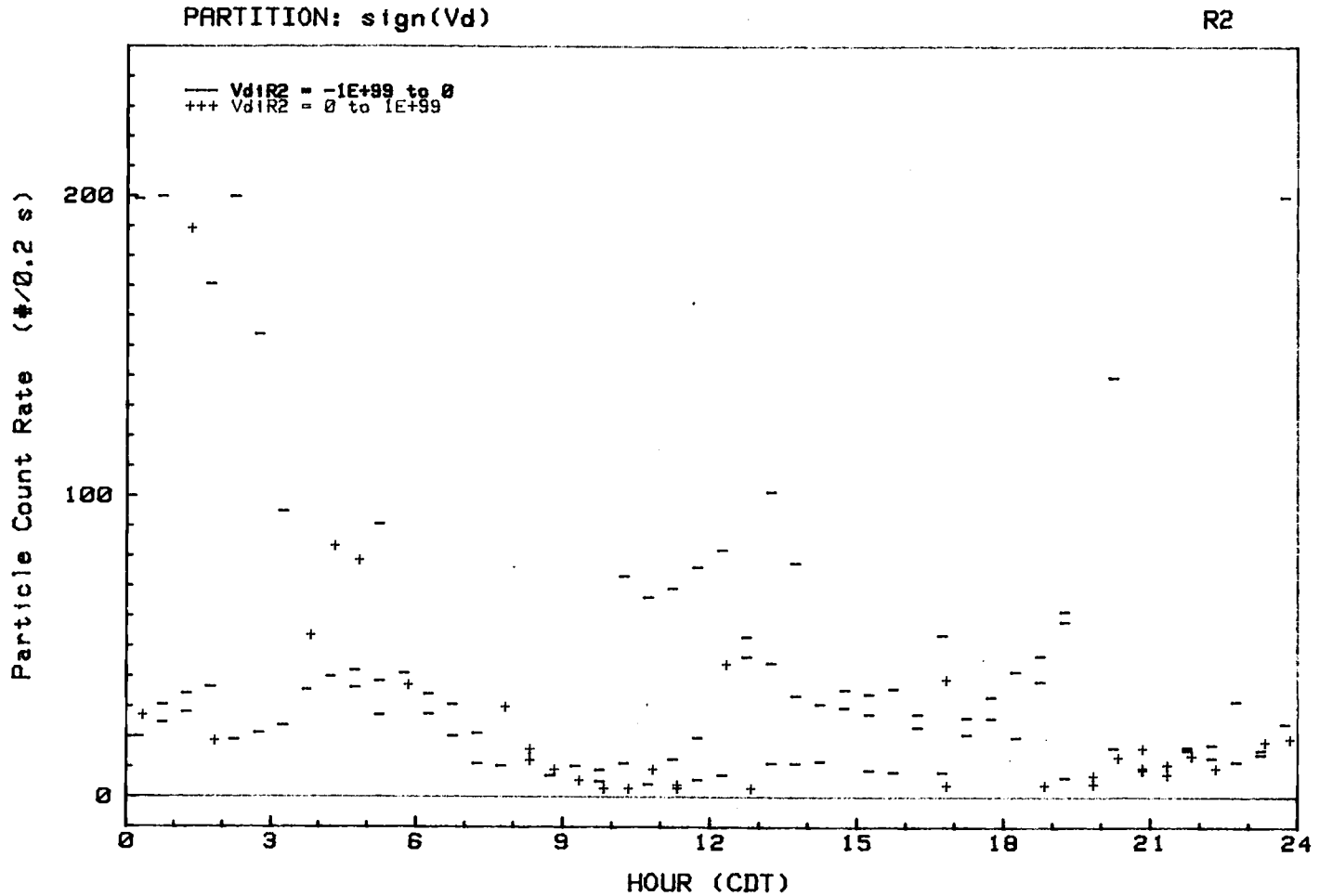

Figure 3.4d: Diurnal composite of particle count rate (R2), partitioned by sign of v_d.

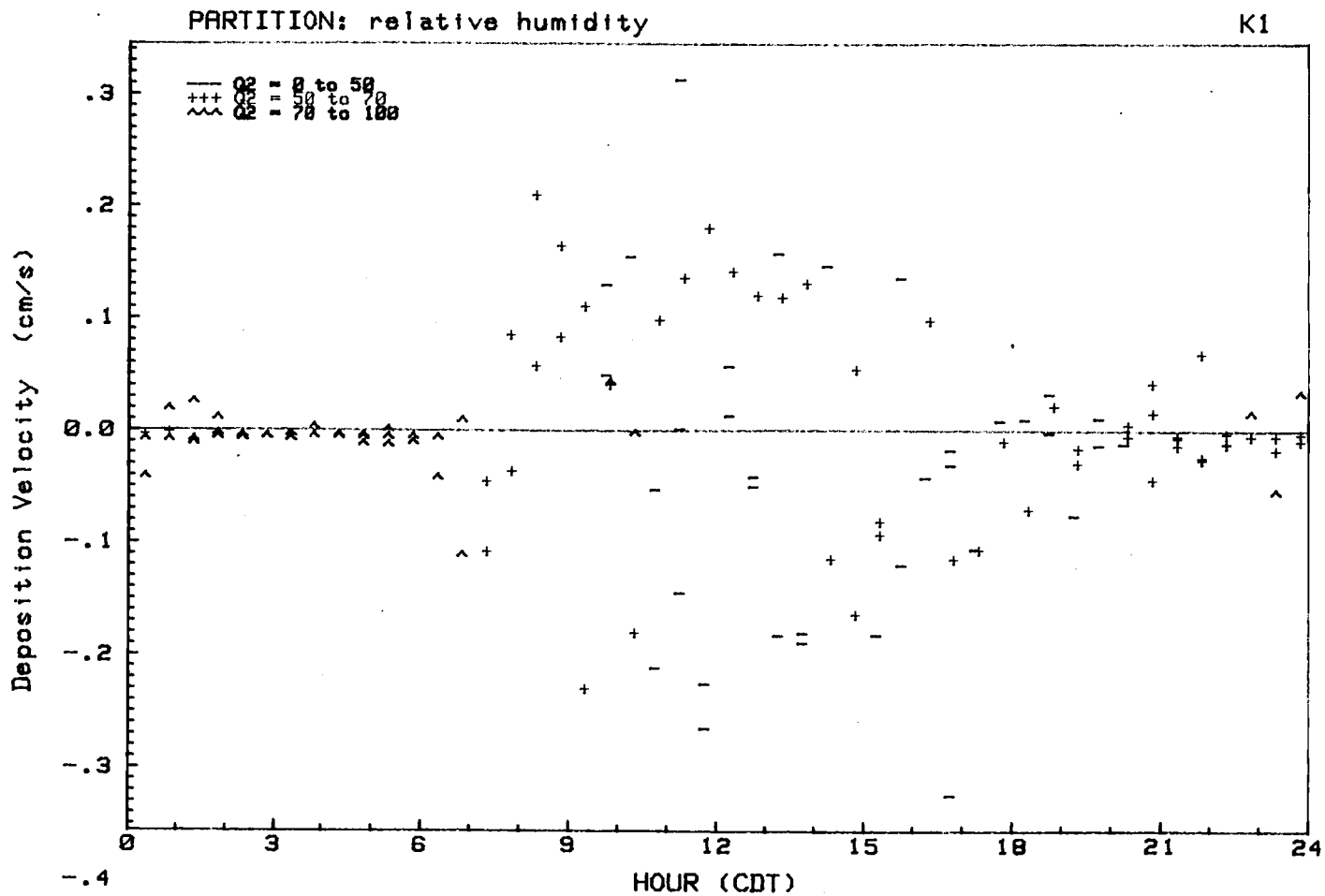

Figure 3.5a: Diurnal composite of deposition velocity (K1), partitioned by relative humidity.

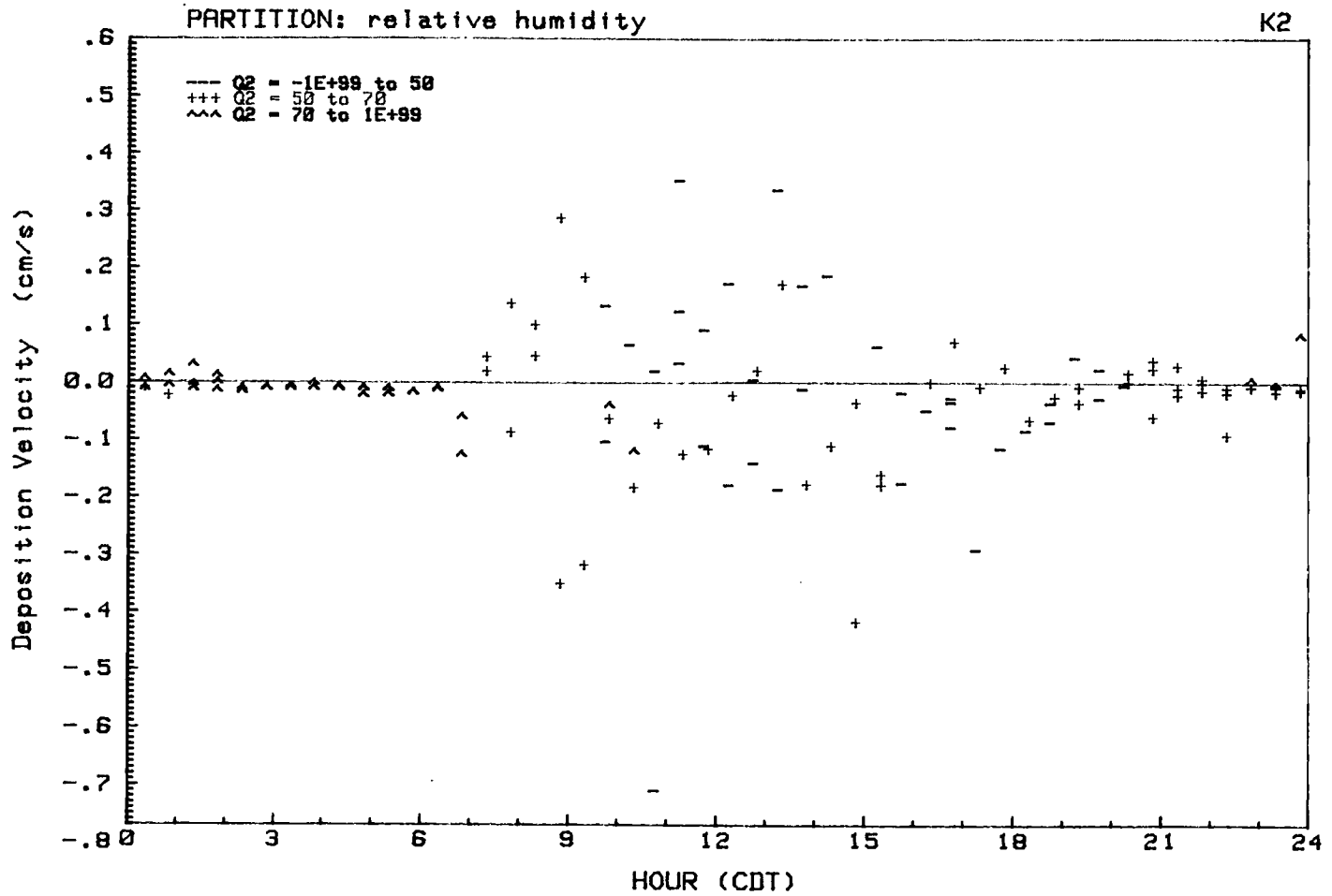

Figure 3.5b: Diurnal composite of deposition velocity (K2), partitioned by relative humidity.

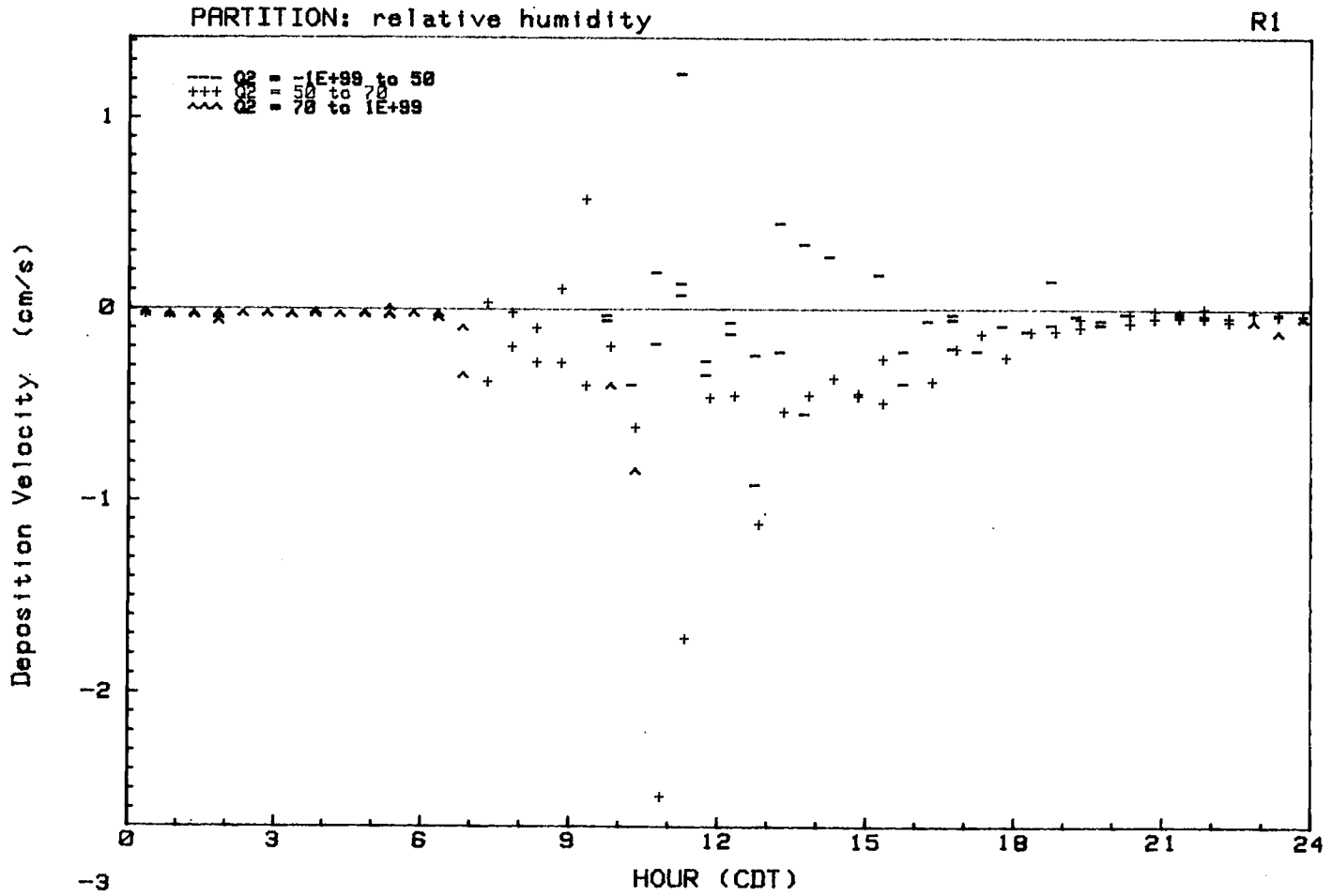

Figure 3.5c: Diurnal composite of deposition velocity (R1), partitioned by relative humidity.

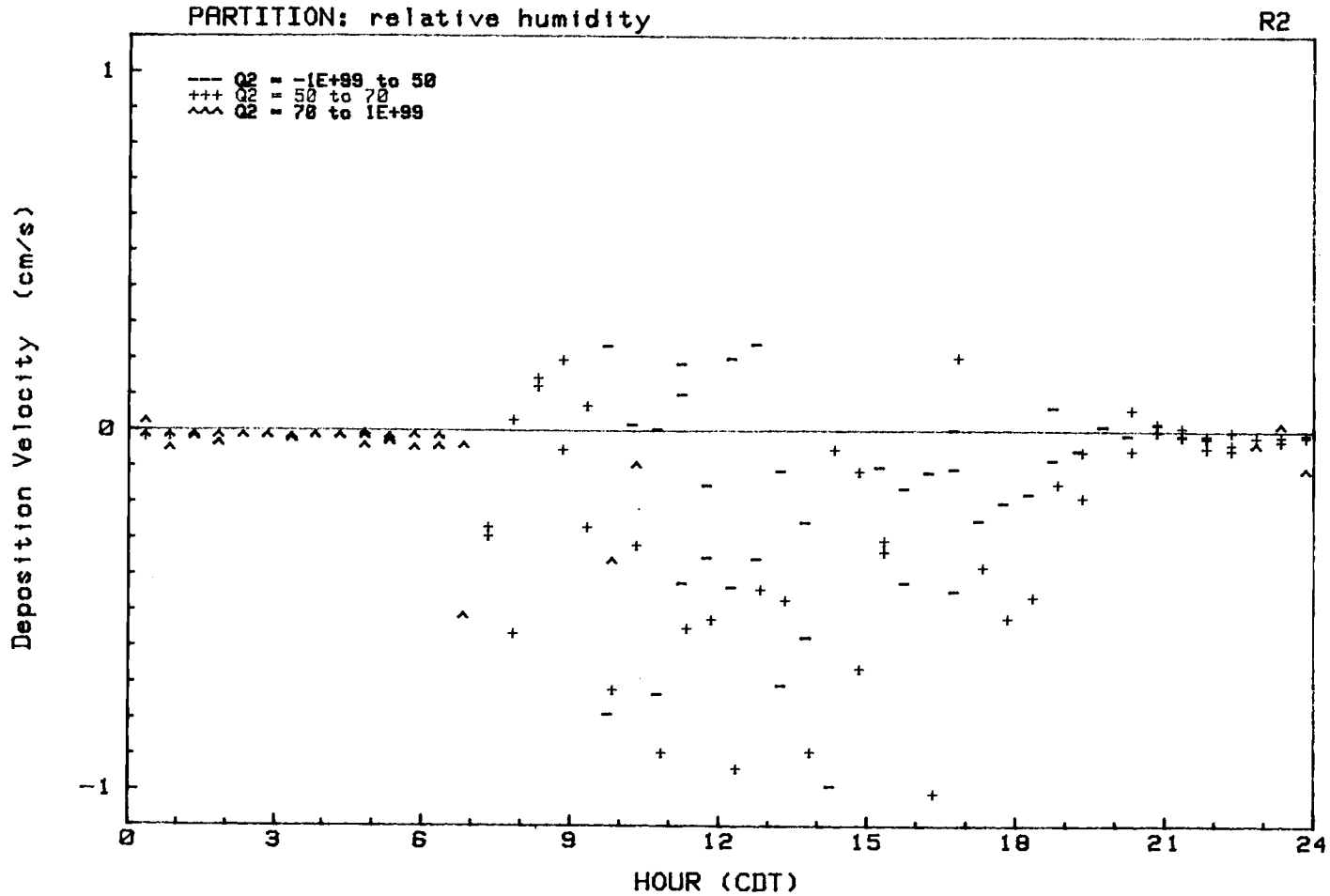

Figure 3.5d: Diurnal composite of deposition velocity (R2), partitioned by relative humidity.

4. ANALYSIS OF VARIANCE

The deposition velocity estimates presented in the previous section exhibit scatter which includes the zero value. This is of concern and raises a question as to the statistical significance of the estimates. One measure of the expected variability due to sampling is the 'standard error' (standard deviation of the sample mean). Calculation of this statistic requires knowledge of the sample distribution of the deposition velocity estimator. Description of this distribution requires an understanding of the random variables which make up the estimator. In this section, a statistical model of the particle sensor signals is developed and the sampling variability of the deposition velocity estimates is examined.

4.1 Model

Each of the calibrated particle sensor signals, which as a time series will be represented by s(t), is equal at any instant to the number of particles counted in a specific size range over a specific period (counter reset interval;) so, s(t) is a step function of time. Therefore, when it is digitized at a sample frequency equal to the inverse of the reset interval, a counting variable is generated. Since this variable is generated by counting particles in a sample volume of fixed size and the particles may be considered to be randomly distributed (on this space scale) it represents a Poisson process (DeGroot, 1975.) If the ambient particle concentration was constant, over the scales of turbulent transport, then s(t) would represent a

HOMOGENEOUS Poisson process (DeGroot, 1975; Haight, 1967). This would be written,

$$s(t) \approx P_T(c), \tag{4.1}$$

and read, "s(t) is distributed as a Poisson variable defined for the counting period T and with a constant distribution parameter, c." However, for the surface layer in which there is a non-zero vertical Reynolds flux of particles, the concentration is not constant over the turbulent scales; indeed it is the variability which indicates a flux if it is correlated with the vertical velocity. Therefore, s(t) is a NON-homogeneous Poisson process,

$$s(t) \approx P_T(c(t)), \tag{4.2}$$

in which c(t) is the variable distribution parameter and also the quantity of interest in computing the Reynolds flux (through its proportionality to concentration.)

If it is assumed that the variability in c(t), the variance σ_c^2, is independent of the Poisson counting variability about c(t), the variance σ_p^2, and that σ_c^2 and σ_p^2 are constants then σ_s^2 may be decomposed according to

$$\sigma_s^2 = \sigma_c^2 + \sigma_p^2. \tag{4.3}$$

This indicates that it may be advisable to model the particle count as the sum of a homogeneous Poisson random variable, p(t) and a second

random variable, c(t), independent of the first and containing the turbulence scale information as

$$s(t) = c(t) + p(t). \tag{4.4}$$

The validity of these assumptions is indicated in part by the relative magnitudes of the component variances in the following way. If σ_p^2 is constant (most importantly, not a function of c(t)) then the independence of c and p is assured. Now, if σ_p^2 is large compared to σ_c^2 then σ_p^2 is, in the worst case, only a weak function of c(t) and therefore practically constant.

In order to compare the magnitudes of the components σ_c^2 and σ_p^2 it is advantageous to review several fundamental properties of the homogeneous Poisson distribution. The population mean E(p) and population variance Var(p) are equal in magnitude to the distribution parameter c. Since the sample estimators of the mean and variance,

$$\bar{s} = \sum_{i=1}^{n} s_i \tag{4.5}$$

and

$$\overline{s'^2} = \sum_{i=1}^{n} (s_i - \bar{s})^2 , \tag{4.6}$$

are unbiased estimators of the population mean and variance respectively, $\bar{s}$ may be used to estimate σ_p^2.

Thus, even though it does not constitute an independent estimate, σ_c^2 may be calculated as the residual of σ_s^2 and σ_p^2, ie,

$$\sigma_c^2 = \sigma_s^2 - \bar{s}. \qquad (4.3b)$$

Finally, then, if σ_p^2 is shown to be large compared to σ_c^2, the simple model may be used to decompose the variance of s(t).

4.2 Data

Before the model may be utilized, its assumptions must be shown to be validated by the data. Figure 4.1 is a scattergram of variance vs. mean for the K1 and K2 signals; it has two important features. First, the location of the majority of the points below a line of slope one must be explained in terms of signal processing if the Poisson model is to be used, otherwise the residual, σ_c^2, would be negative in some cases. If this can be done then the second feature, a hard lower bound in the scatter, immediately suggests itself as the slope of the attenuation factor. That is, the slope of this hard lower bound apparently indicates the limiting case as σ_c^2/σ_p^2 goes to zero and the counting variabliity entirely dominates the particle signal variance.

The variances of Figure 4.1 are attenuated because of rolloff at the high frequency end of the power spectum due to analog low pass filtering, which was applied to all analog signals, as is shown in Figure 4.2. The rolloff in Figure 4.2 is also due to computation of the spectrum to twice the Nyguist frequency of the OPC signal. Examination of a large number of particle signal power spectra from this experiment indicates that the high frequencies are always

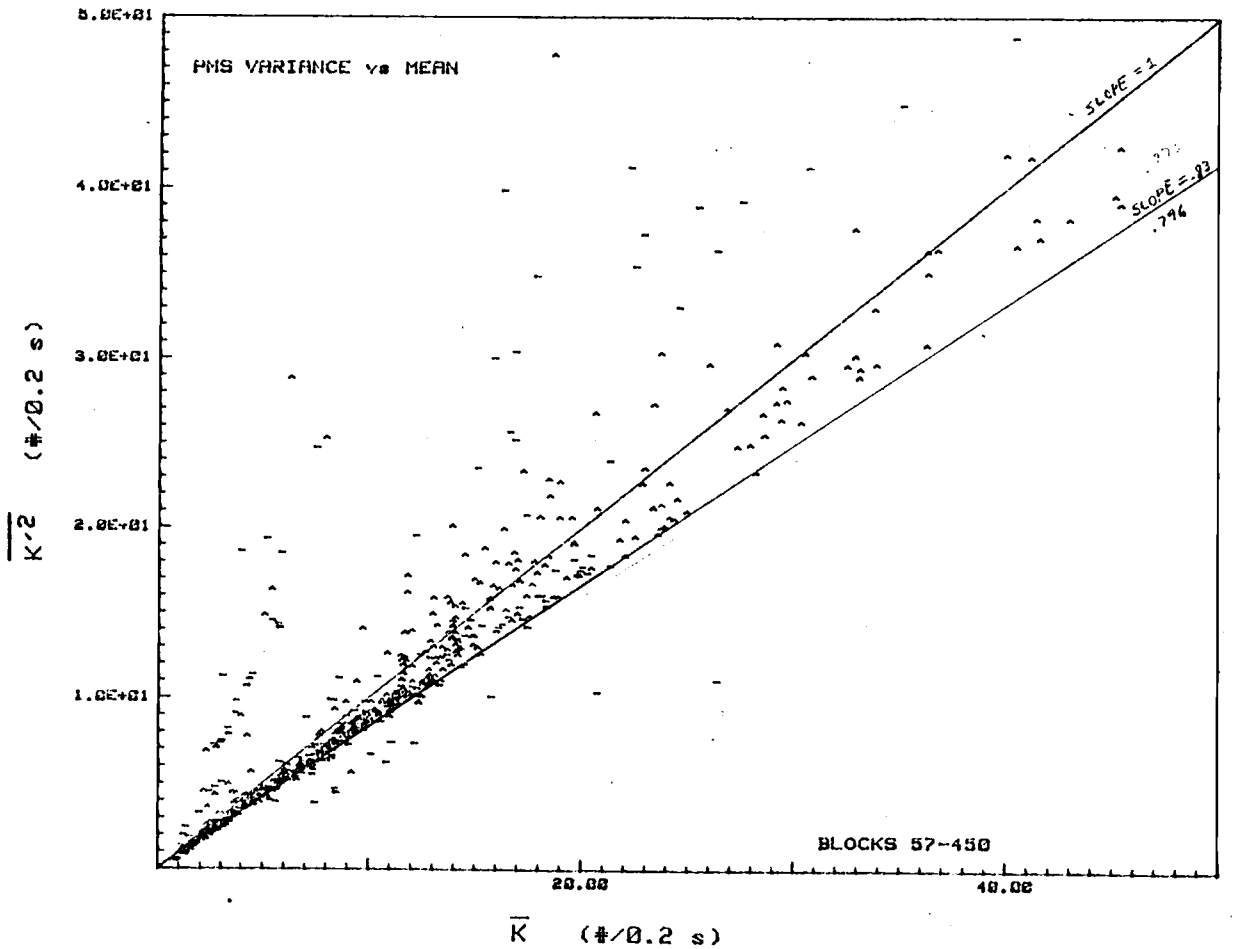

Figure 4.1: Scattergram of raw block variance and block mean for ASAS-300A count rate.

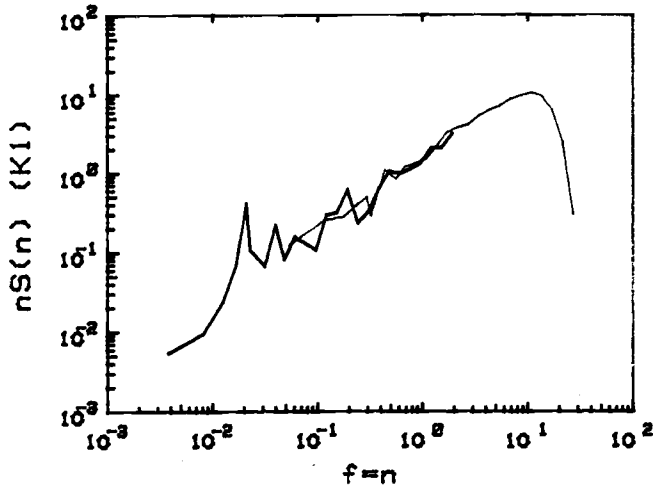

Figure 4.2
Particle signal power spectrum ASAS-300A (K1)

dominated by the white noise due to counting statistics. In light of this observation, a possible correction of the unwanted attenuation is an extrapolation (integration to the Nyquist frequency) of a spectral density which is representative of the white noise portion of the spectrum. This is a relatively computation intensive method which was used for a selected few case studies. The bulk of the K1 and K2 variances were corrected by a simple multiplicative factor based on the hard lower bound in the scattergram of Figure 4.1 as suggested above.

Figure 4.3 is a similar scattergram except it represents the particle signals R1 and R2. The lower bound of the variances is less pronounced and neither is there a significant number of raw variances below their respective mean values. A typical sample power spectrum for the Royco sensor is given in Figure 4.4. Since considerably more non-counting variability is apparent in the lower frequencies, use of the same multiplicative constant that was used for K1 and K2 corrections is not judged as satisfactory. No correction at all may give an estimate which is just as valid.

The model assumption are now examined in light of the partitioned variances. Table 4.1 contains averages over the experiment of the three terms in Equation 4.3 and the ratio of σ_c to σ_p for the four particle sensor signals. The small ratios for K1 and K2 signals are in support of the proposed model of the variances. That is, on the order of 80% of the signal variance is due to Poisson counting. Furthermore, these small ratios suggest the use of an even simpler model of the particle signal variance in the initial formulation of the sample variance of the deposition velocity estimator, at least for the K1 and

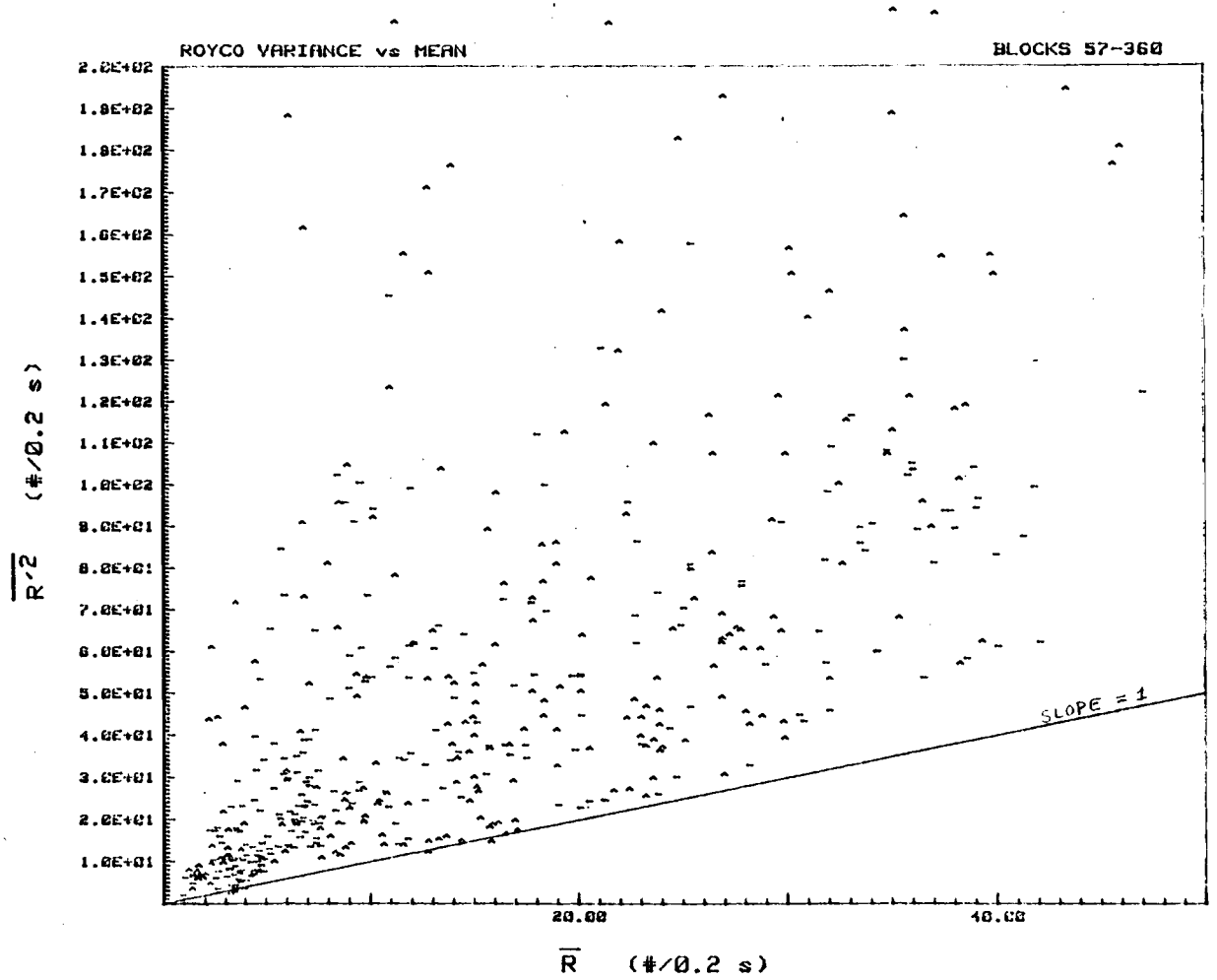

Figure 4.3: Scattergram of raw block variance and block mean for Royco count rate.

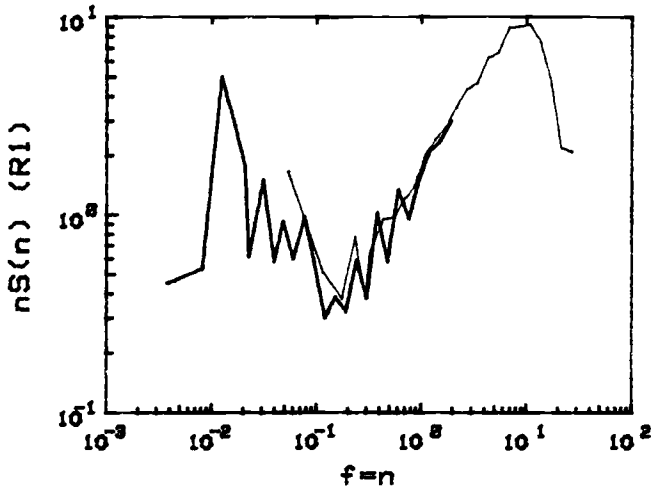

Figure 4.4
Particle signal power spectrum Royco (R1).

Table 4.1
Experimental Averages of Partitioned Variances

Sensor	σ_s^2 (counts^2)	σ_p^2 (counts^2)	σ_c^2 (counts^2)	σ_c^2/σ_p^2	n
K1	25.16	21.4	3.73	0.171	124
K2	16.93	12.6	4.37	0.241	108
R1	117.7	30.0	87.8	3.980	107
R2	83.56	22.3	61.2	3.020	111

K2 results. This simpler model, of course, merely neglects σ_c^2 and estimates σ_s^2 by σ_p^2 (i.e., $\overline{s}$).

Given that σ_s^2 may be estimated by σ_p^2, a formulation of the "standard error" or sample variability of the deposition velocity is proposed based on a homogeneous Poisson model of the particle signal. The most important assumption which is allowed by this model is the independence of p'(t) and w'(t). As previously, the primed notation refers to deviations from the sample mean such that p' and w' are zero mean quantities.

The standard error formula will be derived by examining first the sample variances of the instantaneous eddy product, the average eddy product (covariance) and finally the deposition velocity. The independence and zero mean properties allow for the decomposition of the instantaneous eddy product variance into a product of the individual second moments of w' and p' as follows:

$$\mathrm{Var}(w'p') = \mathrm{Var}(w')\mathrm{Var}(p') \tag{4.7}$$

(see e.g. Mood et al., 1963). The sample mean of w'p' is the covariance, $\overline{w'p'}$. The sample variance of $\overline{w'p'}$ may thus be formulated as follows:

$$\mathrm{Var}(\overline{w'p'}) = \mathrm{Var}\left(\frac{1}{n}\sum_{i=1}^{n} w'p'\right) \tag{4.8a}$$

$$= \left(\frac{1}{n}\right)^2 \mathrm{Var}\left(\sum_{i=1}^{n} w'p'\right) \tag{4.8b}$$

$$= \left(\frac{1}{n}\right)^2 \sum_{i=1}^{n} \mathrm{Var}(w'p') \tag{4.8c}$$

$$= \frac{1}{n}\mathrm{Var}(w'p') \tag{4.8d}$$

$$= \frac{1}{n}\mathrm{Var}(w')\mathrm{Var}(p') \tag{4.8e}$$

$$\hat{=} \frac{1}{n}\overline{w'^2}\,\bar{s} \tag{4.8f}$$

in which steps are justified as follows: (4.8-a) the definition of the covariance; (4.8-b) factoring of a constant; (4.8-c) independence of instantaneous eddy products (no auto-covariance of w'p'(t)) by virtue of initial assumption; (4.8-d) assume var(w'p') is a constant; (4.8-e) substitute Equation 4.7; (4.8-f) substitute variance estimators.

However, the deposition velocity estimator is $(\overline{w'p'})/\bar{s}$ which is a quotient of random variables. According to the original assumption, w'p' is a zero mean quantity which could be viewed as a problem since traditional formulations of the variance of a quotient become undefined if either term has zero mean (Mood et al., 1963). However, it is appropriate here to treat $\bar{s}$ as a constant rather than a random variable since its sample coefficient of variation is much larger than that of $\overline{w'p'}$; so the variance of the deposition velocity estimator may be written as follows:

$$\mathrm{Var}\left(\frac{\overline{w'p'}}{\bar{s}}\right) = \frac{1}{\bar{s}^2}\,\mathrm{Var}(\overline{w'p'}) \tag{4.9a}$$

$$= \frac{1}{n\bar{s}^2}\,\mathrm{Var}(w')\mathrm{Var}(p') \tag{4.9b}$$

$$= \frac{1}{n\bar{s}}\,\mathrm{Var}(w') \tag{4.9c}$$

$$\hat{=} \frac{\overline{w'^2}}{n\bar{s}} \tag{4.9d}$$

in which the final equivalence is read, "will be estimated by."

Finally, the standard error may be written as

$$SE(\hat{V}_d) = \left(\frac{\overline{w'^2}}{n\bar{s}}\right)^{1/2} \tag{4.10}$$

in which V_d represents the estimator of deposition velocity.

This has been calculated for all of the blocks presented in Figure 3.5; diurnal composites are presented in Figures 4.5a-d. Note first the strong diurnal cycle which is due primarily to the square-root dependence on $\overline{w'^2}$ which has a strong diurnal cycle. This effect would be slightly enhanced if the concentration indeed displayed a diurnal cycle maximizing at night. The majority of midday values range from 0.05 to 0.1 cm/s for K1; 0.6 to 1.4 cm/s for K2; 0.2 to 2 cm/s for R1 and 0.2 to 1.3 for R2.

Based on the assumption of independence made at the outset, SE is most valid as a test statistic for the null hypothesis of zero covariance. In view of this, an hourly average envelope of SE about zero is superimposed on the analog derived deposition velocities in Figures 4.6a-d. The figure illustrates that the majority of the values are marginally significant over the standard error; if the 5% level is

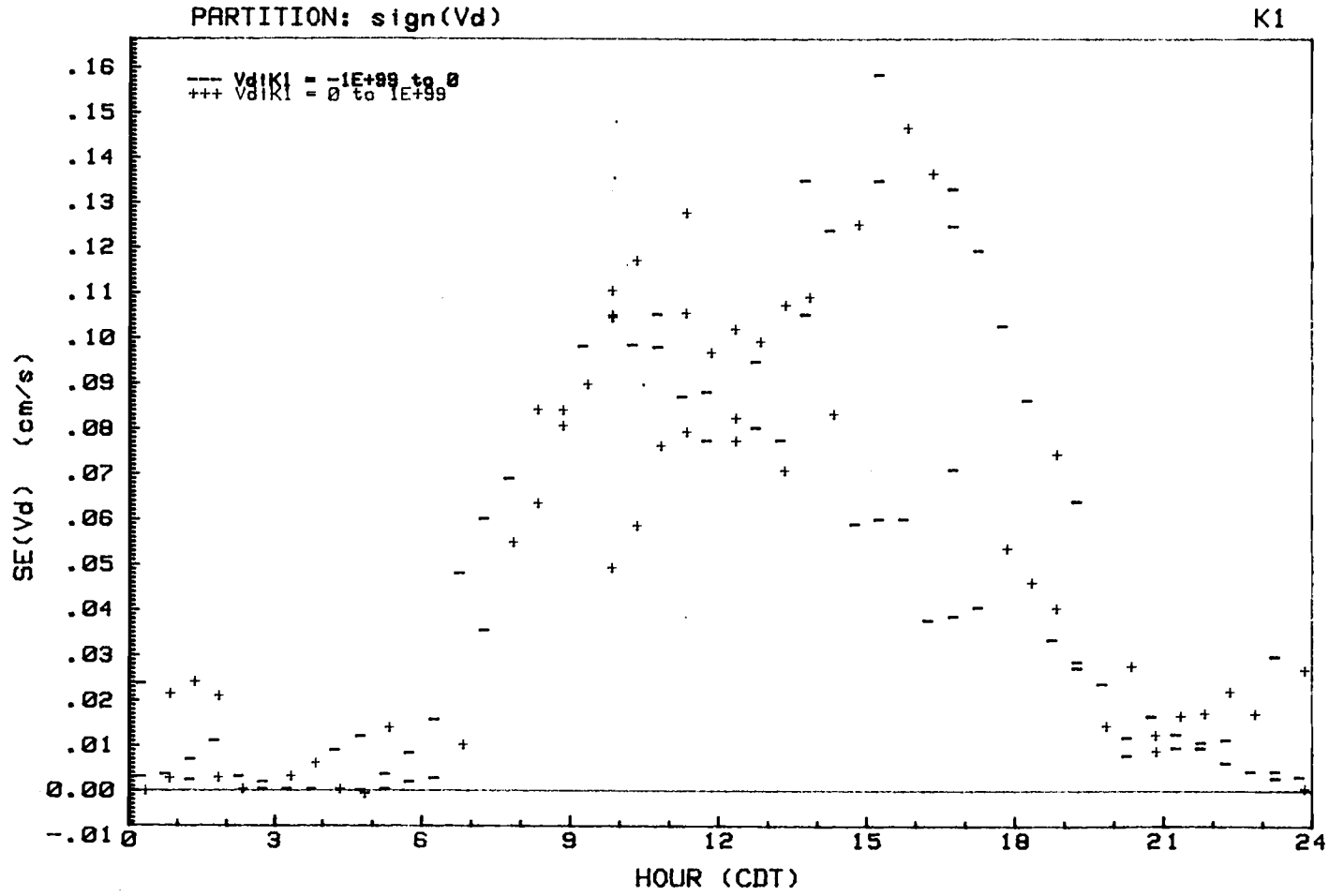

Figure 4.5a: Diurnal composite of the standard error of the deposition velocity estimate (K1).

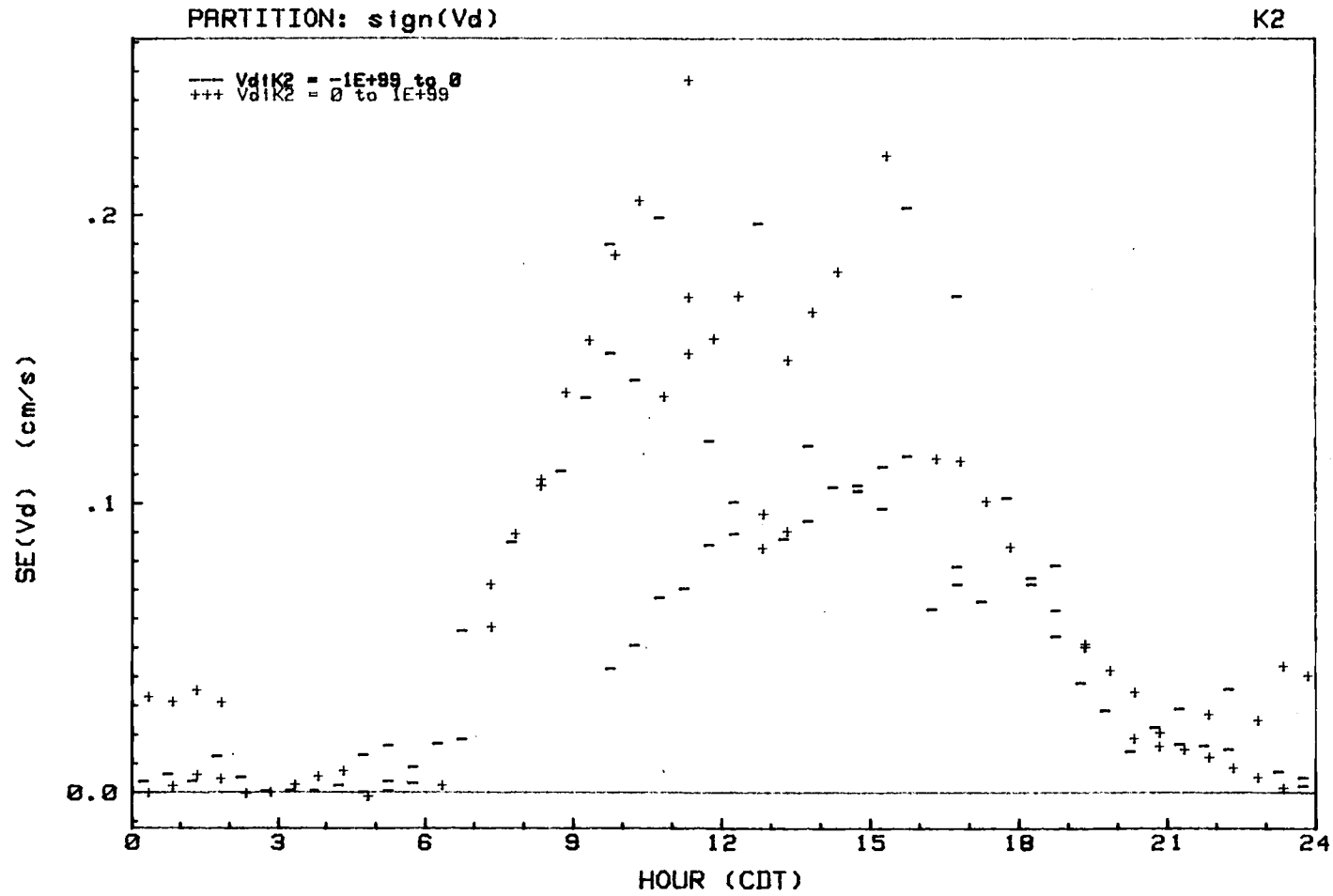

Figure 4.5b: Diurnal composite of the standard error of the deposition velocity estimate (K2).

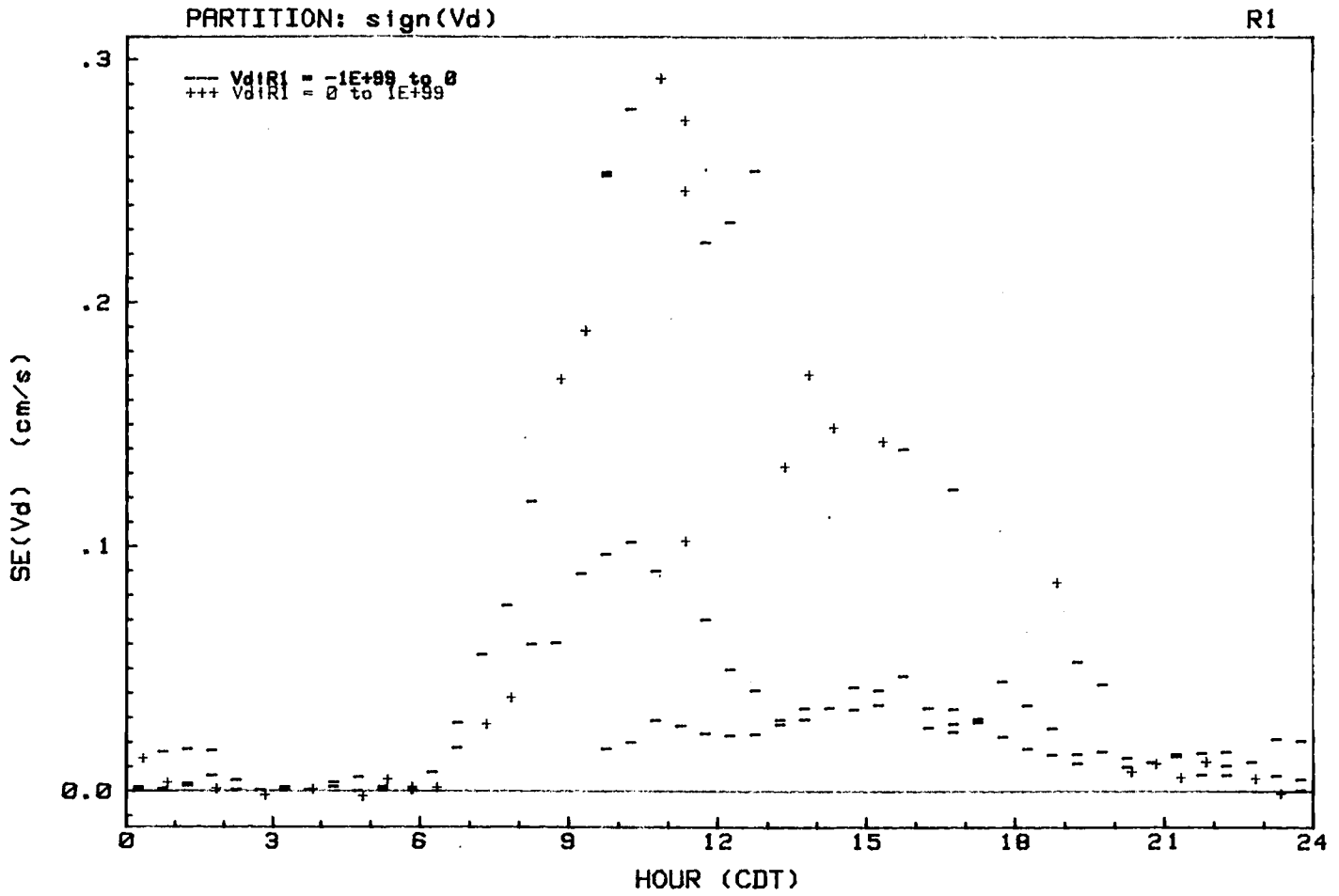

Figure 4.5c: Diurnal composite of the standard error of the deposition velocity estimate (R1).

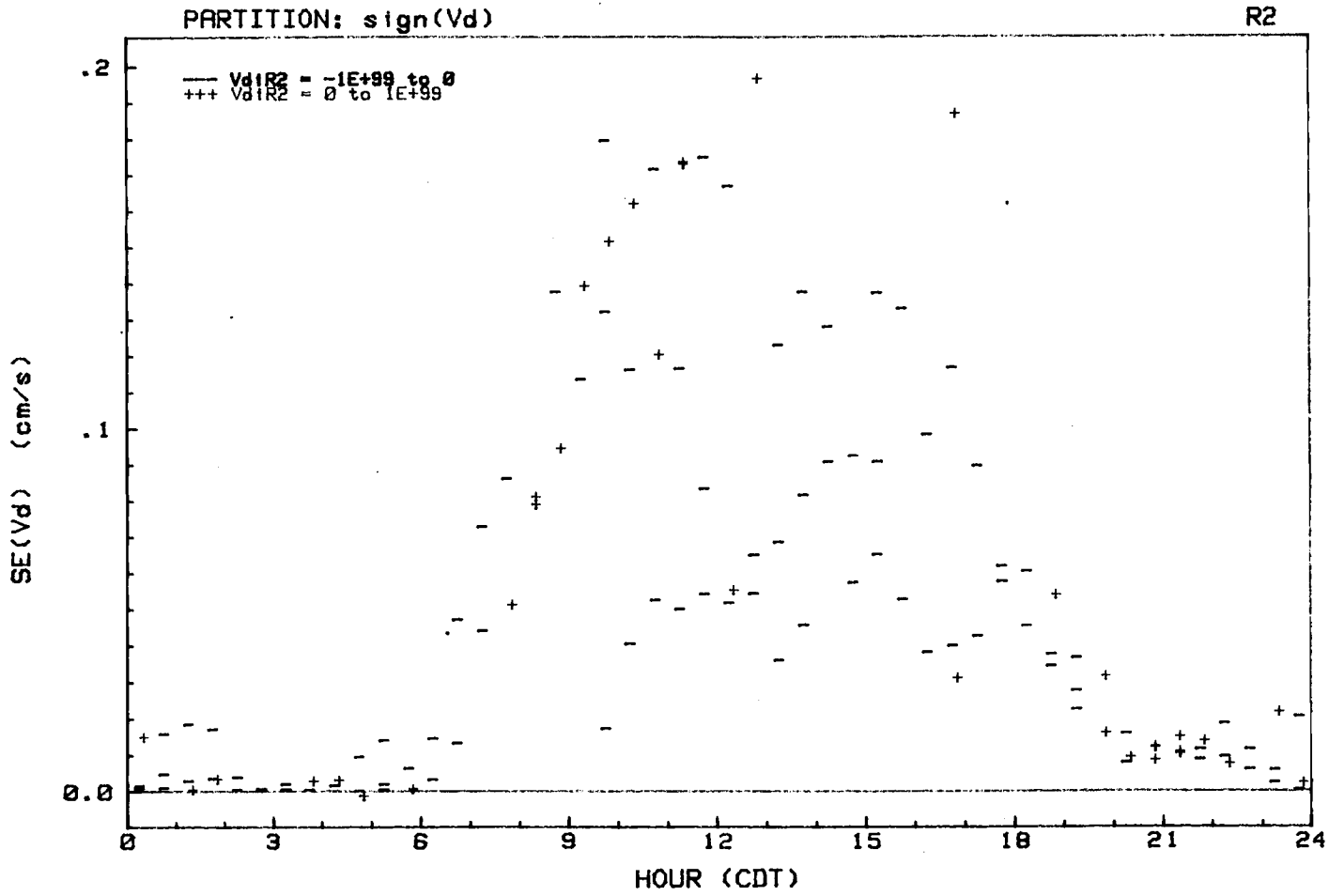

Figure 4.5d: Diurnal composite of the standard error of the deposition velocity estimate (R2).

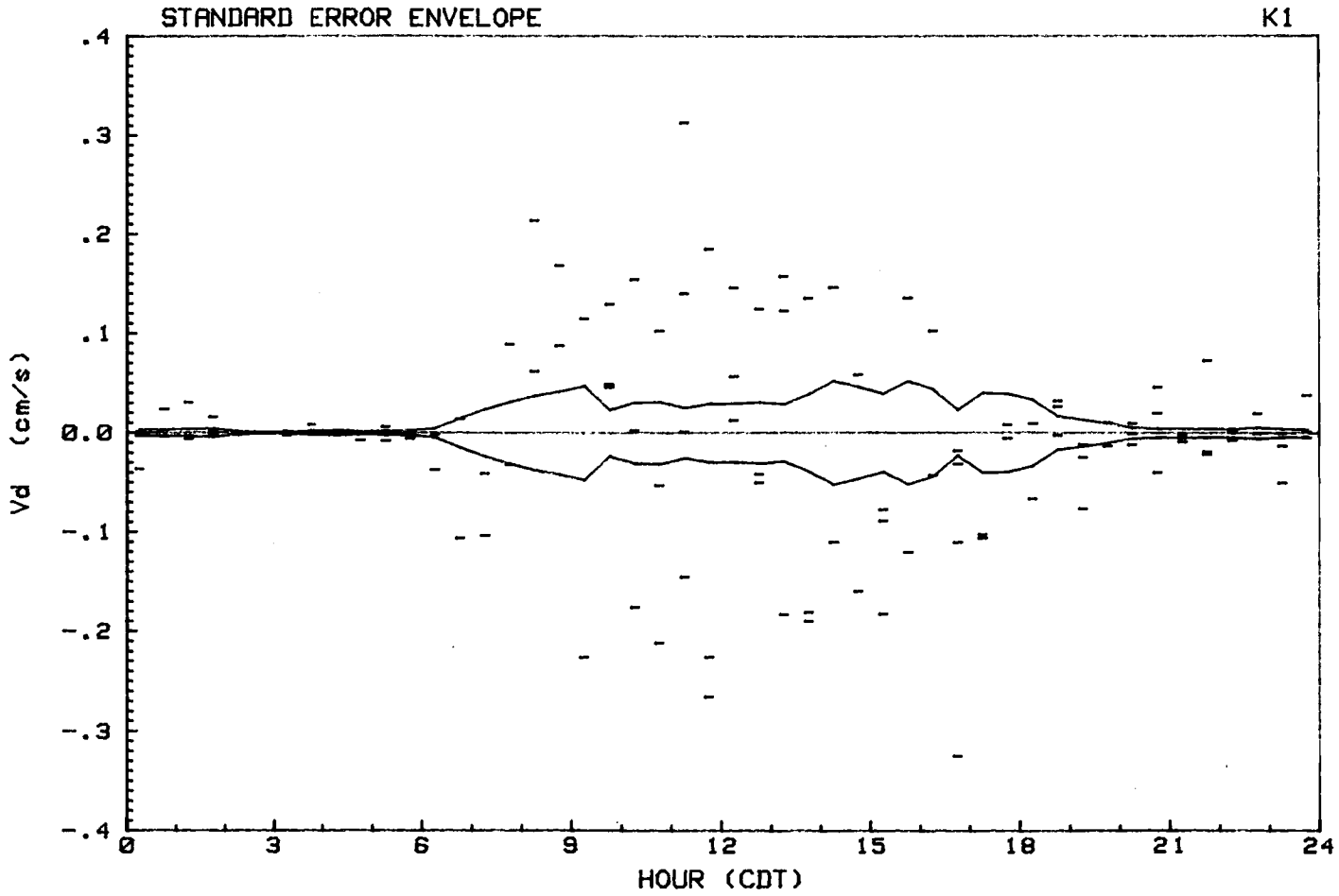

Figure 4.6a: Diurnal composite of deposition velocity (analog estimate) with standard error envelope (K1).

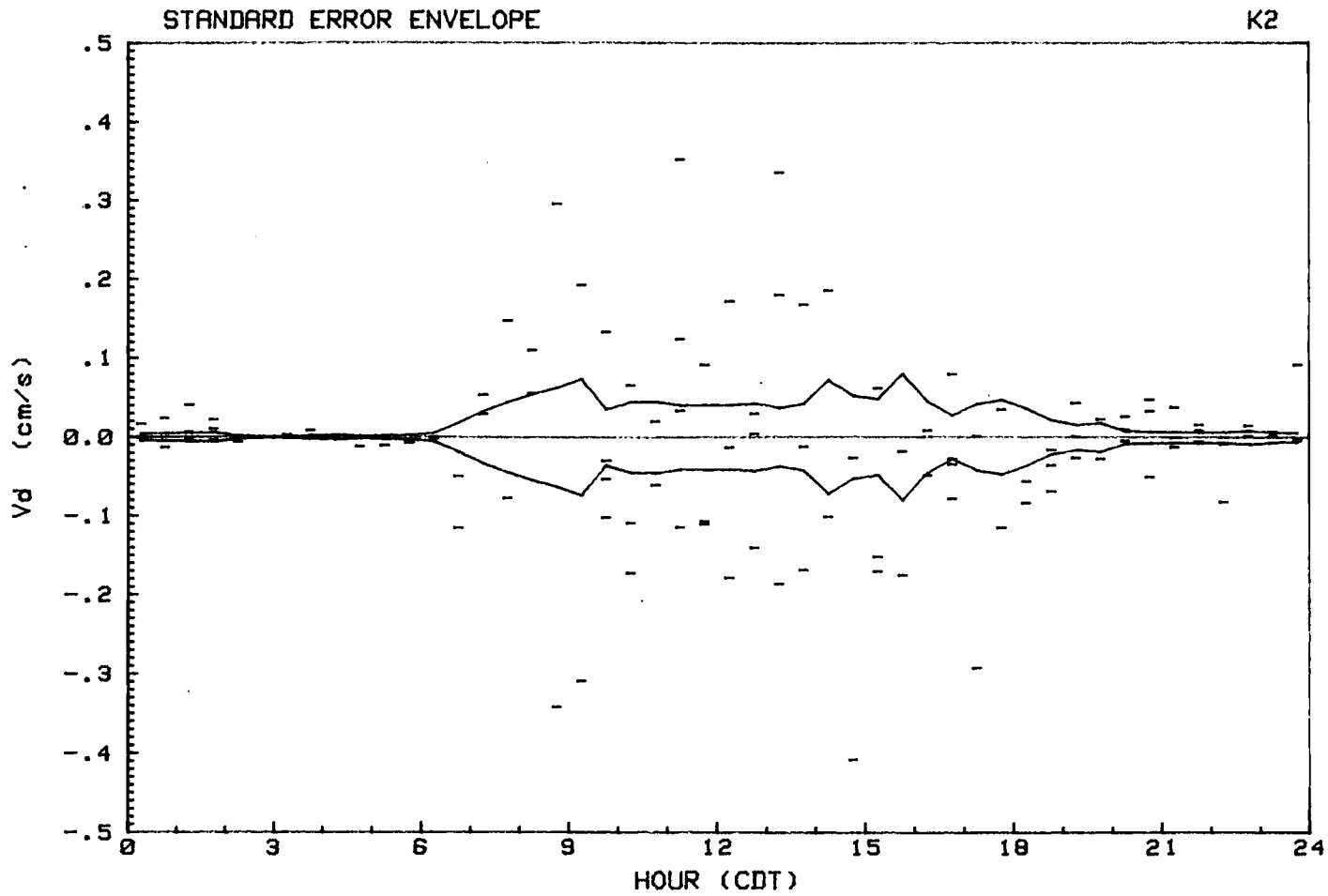

Figure 4.6b: Diurnal composite of deposition velocity (analog estimate) with standard error envelope (K2).

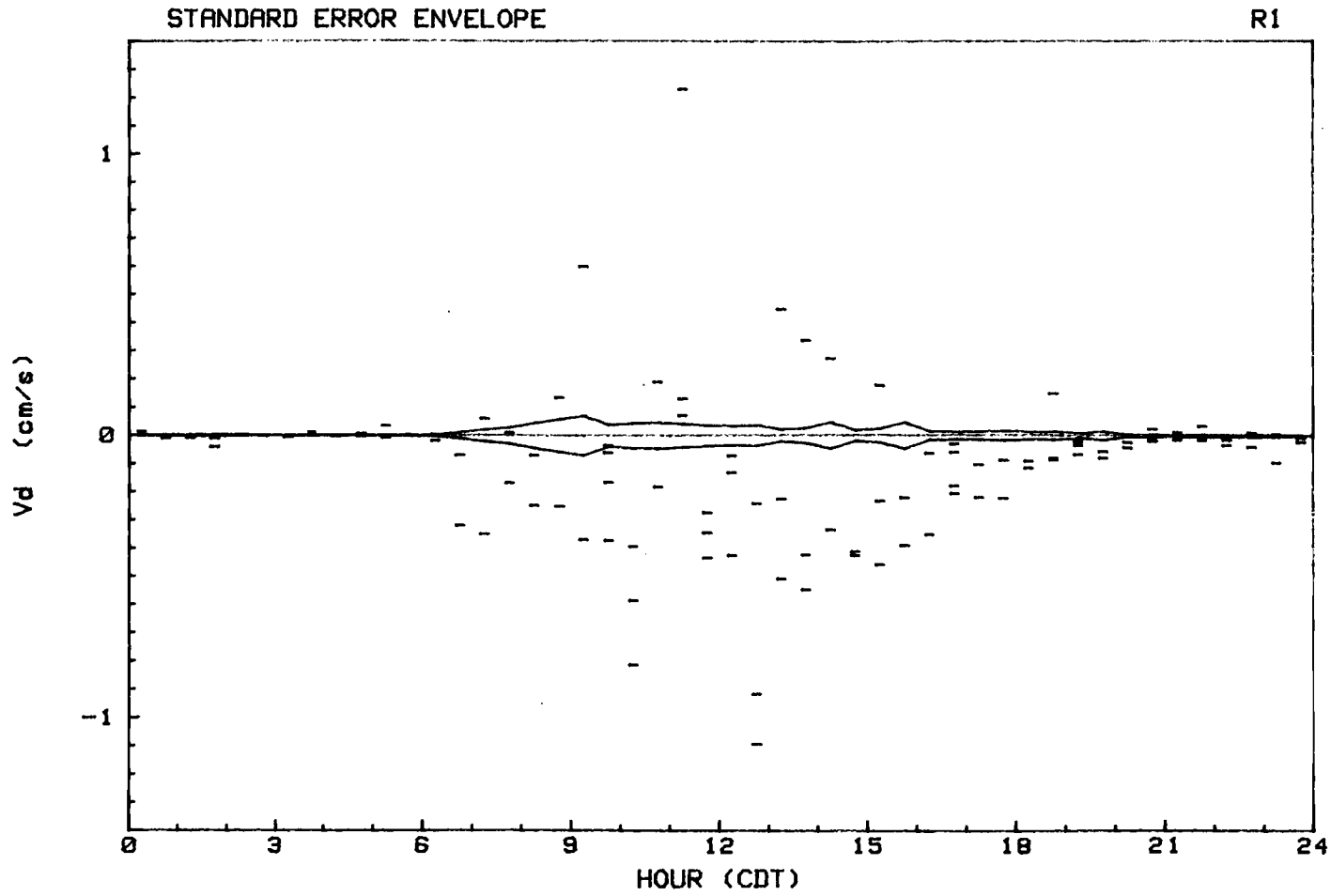

Figure 4.6c: Diurnal composite of deposition velocity (analog estimate) with standard error envelope (R1).

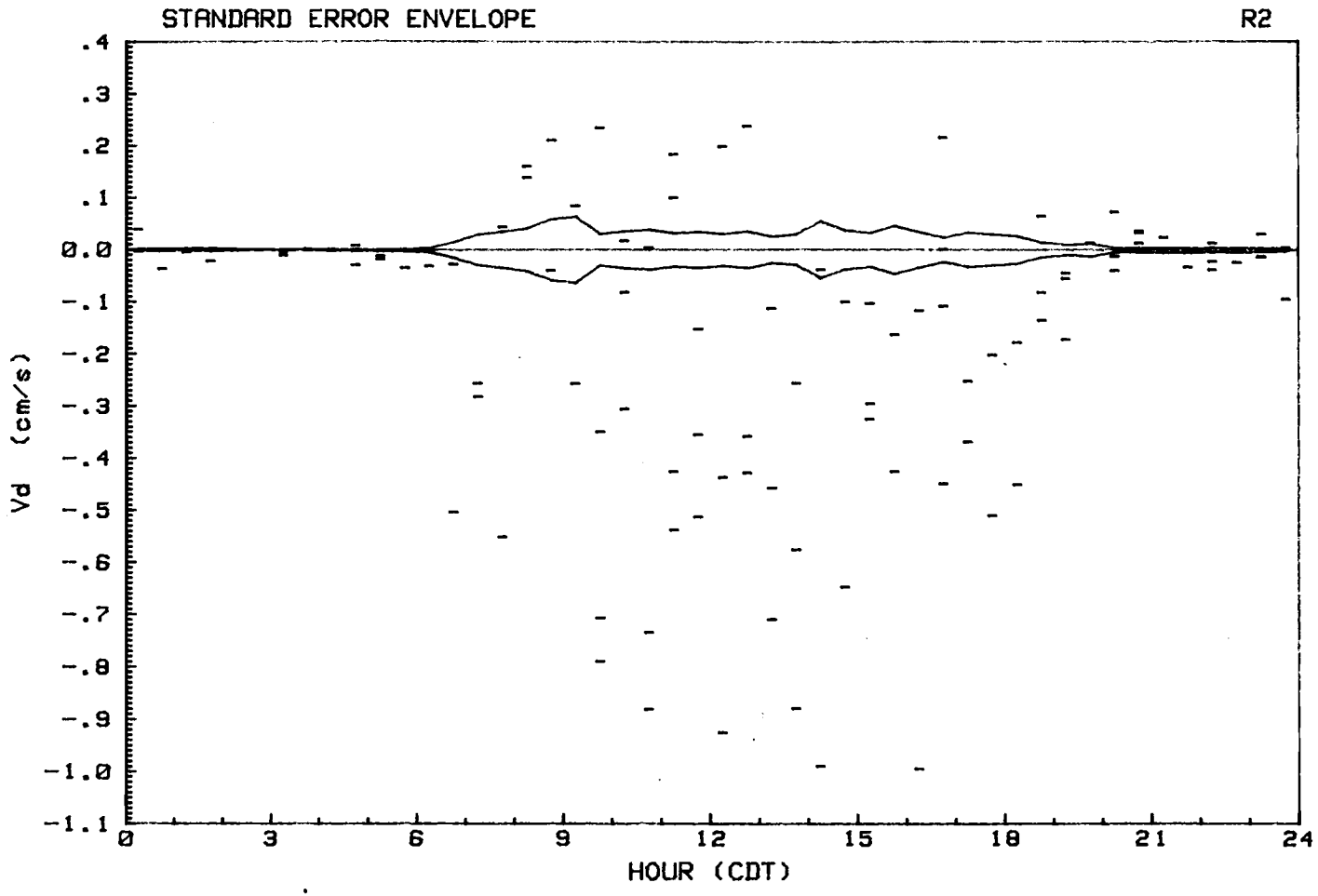

Figure 4.6d: Diurnal composite of deposition velocity (analog estimate) with standard error envelope (R2).

used (1.96*SE is a common hypothesis test statistic) even fewer are significant.

The implications of this result fall into two categories, interpretation of the current data set and design considerations for future experimentation. In terms of the current deposition velocity estimates, the implications must again be categorized, this time according to particle sensors (size ranges.) For the ASAS-300A results (.15<D<0.30 μm), this standard error envelope may be viewed as a nominal upper bound on the magnitude of v_d since the values are only marginally significant and they do not indicate a dominant direction of the flux. However, even the determination of an upper bound is an important result given the current controversy on the subject. Although not shown by Figures 4.6a-b, the half hour averages of v_d that make up these composites also vary about zero in time.

Regarding the Royco results (0.30<D<2.50 μm), the majority are statistically significant according to this error formulation and the dominant flux direction is upward. Due to the upward sense of these values, they will not be used to infer deposition velocities but they will be examined for other information in a subsequent section.

In terms of improving the method, the standard error is too large, by about an order of magnitude for K1 and K2, to resolve deposition velocities as small as 0.1 cm/s to within 10%. Recalling Equation 4.10, it can be seen that, given a constant σ_w^2, SE can be reduced either by increasing n without reducing $\bar{s}$ or by increasing $\bar{s}$ without reducing n. If the sample averaging period (25 minutes in this case) is to remain unchanged, in the interest of stationarity, then the increases may be achieved in two ways. In the first, n is increased

through a decrease in the reset interval of the particle counter (and therefore the data acquisition interval) with a proportional increase in air flow rate through the sensor (so that $\bar{s}$ remains the same.) In the second, $\bar{s}$ is increased, either by an increase in aspiration rate of the sensor or by working in higher ambient concentrations or both. By the square root dependence on n and $\bar{s}$, increases of two orders of magnitude must be achieved in these parameters if this formulation of SE is to be decreased by one order. Note also that in either case, the instrument must be capable of higher count rates by a factor of 100. For the ASAS-300A, coincidence counting errors become greater than 10% at about 500 counts per second (ASAS-300A operating manual) so the recommended increase is not possible in the current configuration.

5. DISCUSSION OF SELECTED RESULTS

5.1 Momentum flux contamination experiment

The previous discusion may be viewed in the framework of a signal-to-noise ratio problem in which the deposition velocity is the signal which is to be measured and the Poisson variability is noise. The standard error presented indicates that the noise has overwhelmed the signal in many of samples in this data set. Another statistic that can be used to interpret these particle flux data is the correlation coefficient between the vertical wind and the particle count rate.

The following discussion focuses on the correlation coefficient and will draw on previous discussion of partitioning the count rate variance and also on a case study of a short experiment conducted during DDIEx in which a better signal-to-noise ratio was achieved through a stronger signal. This experiment was performed subsequent to (and is available only because of) discovery of an error in configuration of the PMS probe for eddy correlation work. This discussion includes a description of the instrumental configuration and it's significance; a presentation of the data indicating the strength of the signal; a comparision of case results with overall results and finally a discussion of the correlation coefficient.

The ASAS-300A is designed primarily for "in-situ" sampling applications in which fast response is not as important as faithful representation of the size distribution of the aerosol. For this reason, the sample volume is optically defined to be precisely a small

fraction of a comparatively large "wind tunnel like" cavity (of diameter 3.4 cm at its smallest.) The inlet is a 100-to-1 bell-shaped accelerator intended to minimize any size-dependent cross-streamline particle trajectories which would bias the size distribution (these biases occur at an inlet under anisokinetic sampling conditions.) The cavity is aspirated by a "muffin-fan" downstream of the sample volume, and according to PMS, constant flow is achieved to within 1%. In the early portion of DDIEx, the accelerator was separated from the sample cavity by a 1.25 m aluminum extension to minimize flow distortion at the anemometer and it was directed to the south.

This "in-situ" configuration (which will be referred to also as the bell configuration case) was found to be unsuitable for eddy correlation measurements of particle flux because the pressure fluctuations at the accelerator bell, due to horizontal wind variation, cause significant flow rate variations in the sample cavity. These flow rate variations dominate ambient concentration variations and, through their proportionality to a component of the horizontal velocity, contaminate the particle flux with momentum flux as will be shown.

The ASAS-300A can be fitted with a "calibration insert" which reduces the cavity diameter to 2.66 mm which eliminates the momentum flux contamination. In this mode the sensor is aspirated by a pump. The calibration insert with a 1.5 m extension was used for all data presented in this paper (approximately 230 blocks) except for this case study.

For the purpose of examining and documenting the extent of the momentum flux contamination of the bell configuration covariances, a

hotwire anemometer was calibrated and inserted at the center of the inlet extension, as shown in the schematic of Figure 5.1. The hotwire signal, F, was monitored by the analog covariance meter and also stored on digital tape for later analysis. The micro-cup anemometer signal was also monitored by the covariance meter, but was not explicitly digitized. This configuration was sampled for a single 25 minute block. This case study also examines a block, occurring 1/2 hour later in the calibration-insert configuration, which is taken to be representative of the remainder of the experiment. Table 5.1 presents several statistics for these two blocks, which will be referred to as "contaminated" and "uncontaminated" respectively.

A scattergram of two digitized integrator outputs of the covariance meter is shown in Figure 5.2 for the contaminated block; the integral of w'u' is plotted on the abscissa and the integral of w'p' is plotted on the ordinate. Except for a short period at the begining of the block (near (0,0)) the two signals are very highly correlated. This suggests a high degree of contamination by momentum flux of the particle flux measurements.

This case was also examined from the perspective of linear modeling to determine whether concentration variation or flow rate variation dominated the signal variance. Coefficients of determination were calculated for these two blocks and are presented in Table 5.2. In this notation convention, $r^2_{KF|w}$ represents the amount of variance accounted for by the inclusion of F in a model of K when w was already in the model. Note that r^2_{KF} is not only larger than r^2_{Kw}, but it is larger than $r^2_{KF|w}$ as well. This means not only that there is more information regarding the count rate in the sensor

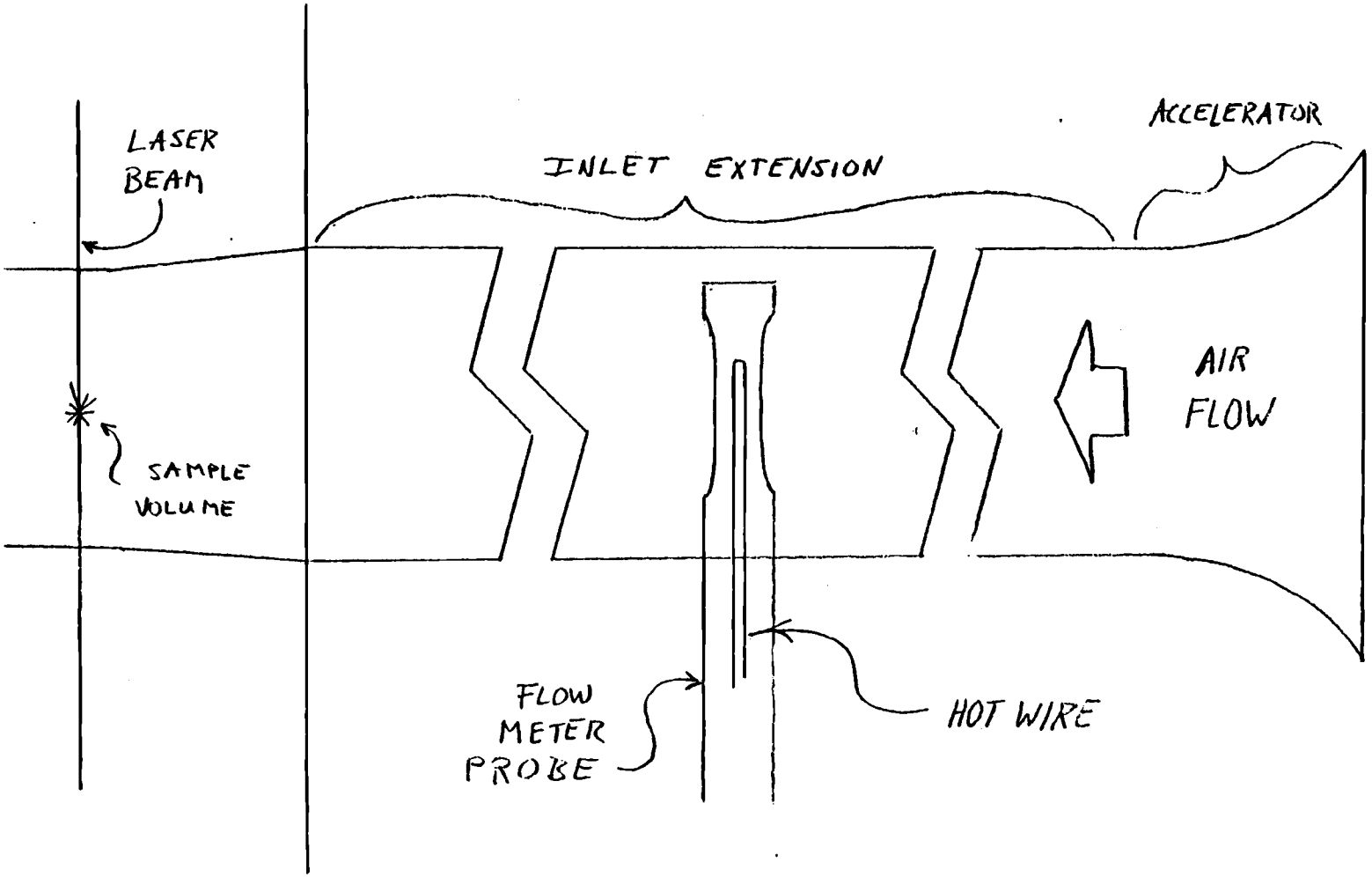

Figure **5.1: Schematic diagram of inlet extension during "bell configuration experiment."**

Table 5.1
Partitioned Variances From Bell Configuration Experiment

Partition	Contaminated	Un-contaminated
σ_s^2	18.060	17.341
σ_p^2	17.453	17.042
σ_c^2	0.607	0.299
σ_p^2/σ_c^2	28.8	57.0

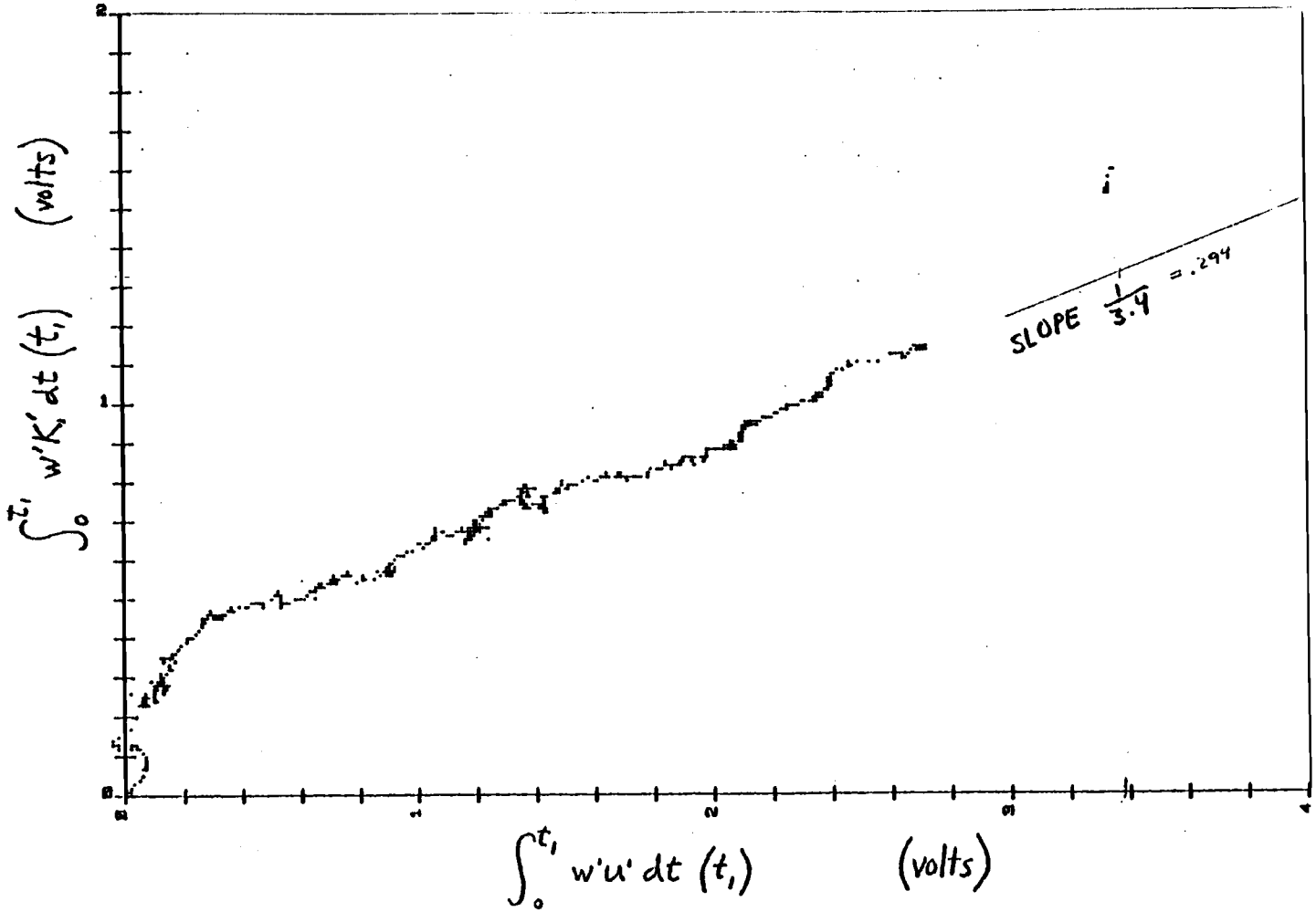

Figure 5.2: Scattergram of covariance meter integrator signals indicating high correlation between momentum flux and "in-situ configured particle flux."

Table 5.2
Coefficients of Determination and Coefficients of Partial Determination for Momentum Flux Contaminated Block

Coefficient	K1	K2
r^2_{Kw}	0.00893	0.00834
$r^2_{Kw\|F}$	0.00025	0.000375
r^2_{KF}	0.0524	0.0443
$r^2_{KF\|w}$	0.0441	0.0365
r^2_{Fw}	0.122	=
$r^2_{Fw\|K}$	0.114	0.115
r^2_{Fw}	-0.350	=

flow rate than in the vertical wind but that there is more ADDITIONAL information. The magnitudes of these coefficients may seem small but recall that the Poisson counting variability plays a large role in the variance of the particle count rate signal, a point which will be treated presently. In light of this, note the much smaller $r^2_{K,w}$ for the uncontaminated case.

As further evidence of momentum flux contamination of the bell configuration covariances, power spectra of the particle signals and co-spectra of the particle signals with the vertical wind signal are presented in Figure 5.3. Also shown, for purpose of comparison with these cospectra is a cospectrum of the micro-cup signal and the Gill propellor signal from a different day.

The particle signal power spectra for both the contaminated and un-contaminated blocks are dominated by the white noise of the Poisson counting variance. The rolloff at high frequencies is due to analog low-pass filtering and in this graph due to plotting frequencies above the K1 Nyquist frequency. The two power spectra differ in the slightly greater amount of non-Poisson variance apparent at the low end of the contaminated spectrum. This observation is verified by the larger value of σ_p^2 (see Table 5.1) in the contaminated over the un-contaminated case.

In contrast to the strong dominance of both power spectra by the Poisson variance, the cospectra exhibit considerable difference. The cospectrum of the contaminated case is very well behaved and exhibits the character of the momentum flux cospectrum also shown. However, the un-contaminated case displays no organized cospectral density over the entire frequency band. These cospectral observations may be

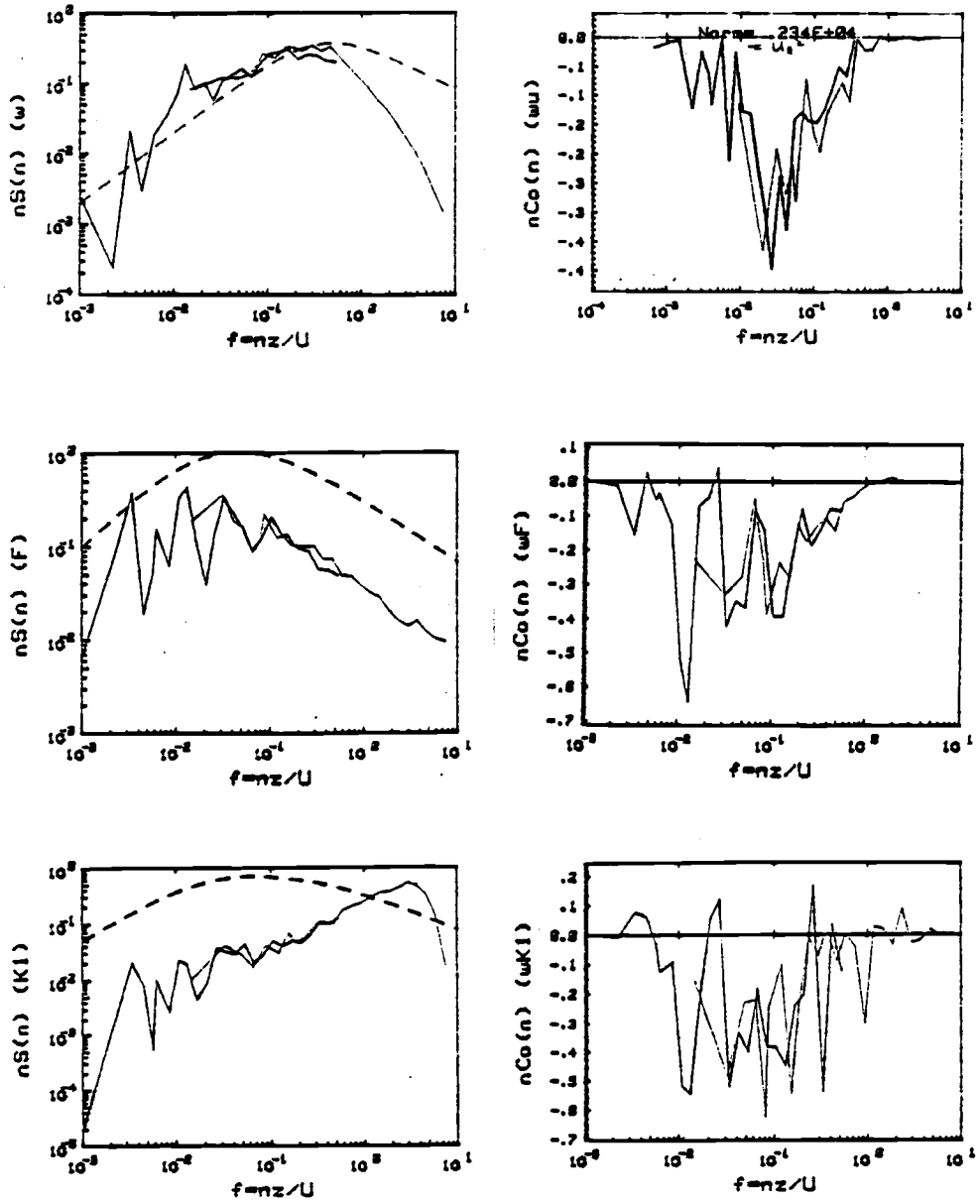

Figure 5.3a:
Signal spectra and cospectra from "bell configuration experiment" contaminated block.

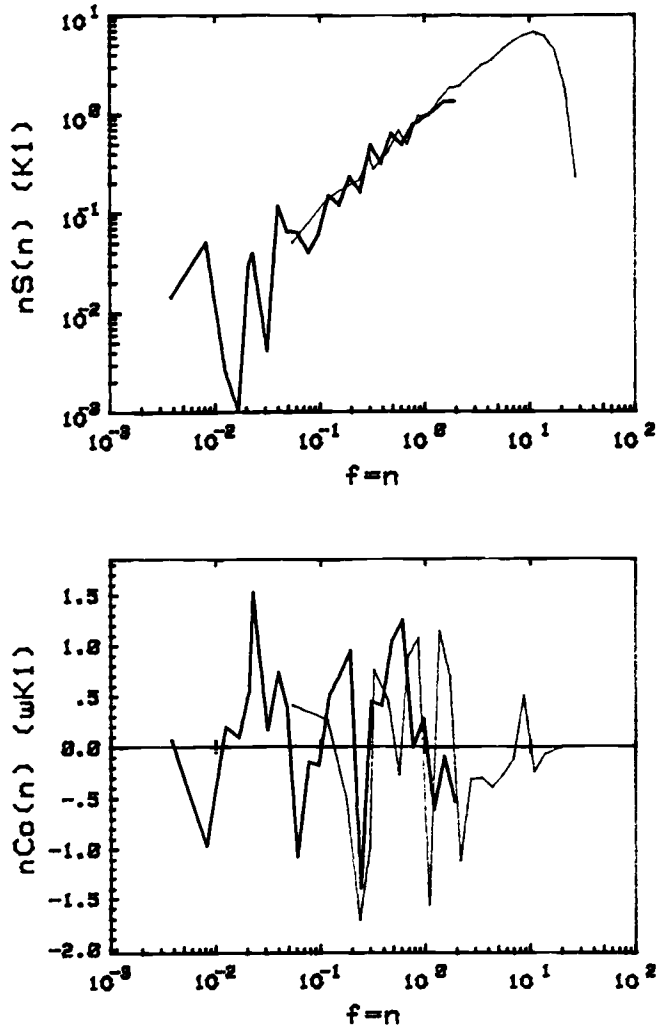

Figure 5.3b. Signal Spectra and Cospectra from "bell configuration experiment" uncontaminated block.

summarized by their integrals, which are the covariances given in Table 5.1.

Since the momentum flux contamination has been shown to dominate the bell configuration covariances, it is interesting to examine the experiment from a different point of view. Consider now that the momentum flux is the quantity of interest and that the particle counter takes the place of a cup anemometer in measuring the fluctuations in horizontal wind. The Poisson counting variance again causes unwanted noise in the signal. The following discussion addresses the question: Is the signal-to-noise ratio tolerable for the purpose of a momentum flux estimate? The tool used to examine the question is the correlation coefficient.

The correlation coefficient is defined according to

$$\rho_{wu} = \sigma_{wu}/(\sigma_w \sigma_u) \tag{5.1}$$

in which the numerator is the population covariance, the denominator is the product of the population standard deviations and the subscripts w and u signify vertical and horizontal wind respectively. This will be estimated from the data by

$$r_{wu} = \frac{\overline{w'u'}}{(\overline{w'^2}\ \overline{u'^2})^{1/2}} \tag{5.2}$$

in which the overbar indicates a sample average and the means of the perturbations are zero. For this discussion, $\overline{w'K1'}$ will be substituted for $\overline{w'u'}$ and the estimate of σ_c^2 $(K1'^2 - K1)$ will be substituted for $\overline{u'^2}$. The latter substitution is justified since it is the natural variability in horizontal wind, not the Poisson counting

variance, which will give a relevant correlation coefficient. Recall that the particle count variances had to be corrected for high frequency rolloff; the method used in this case study is the spectral extrapolation described above.

Correlation coefficients for the contaminated blocks and the uncontaminated blocks are presented in Table 5.3. Also presented are the correlation coefficients that would have resulted from including the Poisson variance in the estimate of σ_u^2 and these are indicated by a star. The variance (σ^2_s or σ^2_c) used to normalize the covariance is indicated. Note first that r_{FK1} is greater than one(1), which implies that the variance was undercorrected for high frequency rolloff. In light of this, r_{wK1} compares very favorably with r_{wF} which is the inlet-hotwire estimate of ρ_{wu}. It also compares favorably with $-r_{wu}$ as calculated from the ANL results for this block, which was 0.27. For the sake of comparison, correlation coefficients of heat flux (r_{wT}) and vapor flux (r_{we}) were both 0.37. Note also that the deposition velocity based on this block is 0.45 cm/s.

The spectral density which was integrated to the Nyquist frequency was rather subjectively chosen to be representative of the white contribution to the spectrum. The residual, σ_c^2, is quite sensitive to this choice so a value of r_{FK1} greater than zero is not really surprizing. Moreover, an iterative correction procedure, that brings r_{FK1} arbitrarily close to unity, might be better than the procedure used. If this were done, r_{wK1} would be reduced in magnitude from 0.41 to 0.35 which is closer to the value based on the micrometeorological sensors.

Table 5.3
Correlation Coefficients From Bell Configuration Case Study

Correlation Coefficient	Variance Used	Contaminated Block	Uncontaminated Block
r_{wK_1}	σ_s^2	-0.075	0.0002
$r^*_{wK_1}$	σ_c^2	-0.41	0.0015
r_{FK_1}	σ_s^2	0.22	---
$r^*_{FK_1}$	σ_c^2	1.18	---
r_{wF}		0.35	---
r_{wu}		-0.27	-0.28
r_{wT}		0.37	0.39
r_{we}		0.37	0.48

The important result here is that the Poisson variance, while large, is well behaved; that is, it is uncorrelated with u' and therefore a reliable estimate of $\overline{w'u'}$ may still be made. However, the signal of interest is w'c' and not w'u'. There are two primary implications of this result, one dealing with the interpretation of the present data set and the other dealing with future use of this type of sensor.

If the correlation coefficient is viewed as a specialized signal-to-noise ratio, this case study suggests that the uncontaminated particle flux covariance is too weak to be resolved through the relatively constant noise level due to the Poisson statistics at these count rates. This is illustrated by the correlation cofficient r_{wK1} for the uncontaminated case, 0.0015, which is given in Table 5.3. This value is so small that it is not statistically significant at the 5% level; a value greater than 0.008 would be required, given the current sample size, n. As stated above, this formulation of a correlation coefficient is highly sensitive to the abitrary correction made for power spectrum rolloff; in this case a 12% decrease in the additive correction of σ_s^2 could bring r_{wK1} up to a significant level (more than a five-fold increase.) The implication here is essentially the same as that of the standard error results of Section (4) but the severity of the problem is more apparent in this framework.

The uncontaminated block was chosen in this case study for its proximity to the bell configuration experiment and not necessarily its representativeness of the data set. However, using the corrected

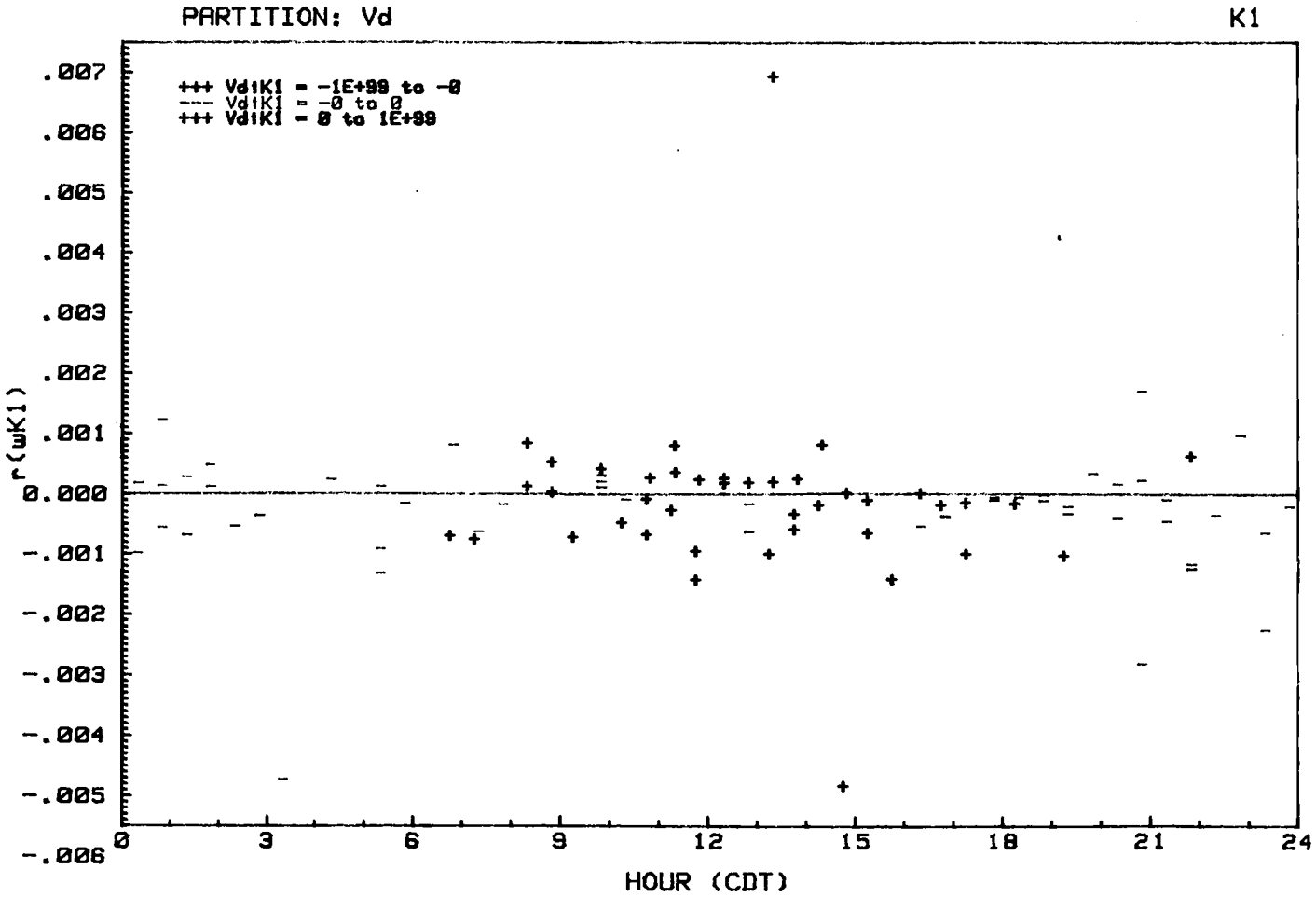

Figure 5.4a: Diurnal composite of w vs. particle count correlation coefficient (K1), partitioned by analog deposition velocity estimate.

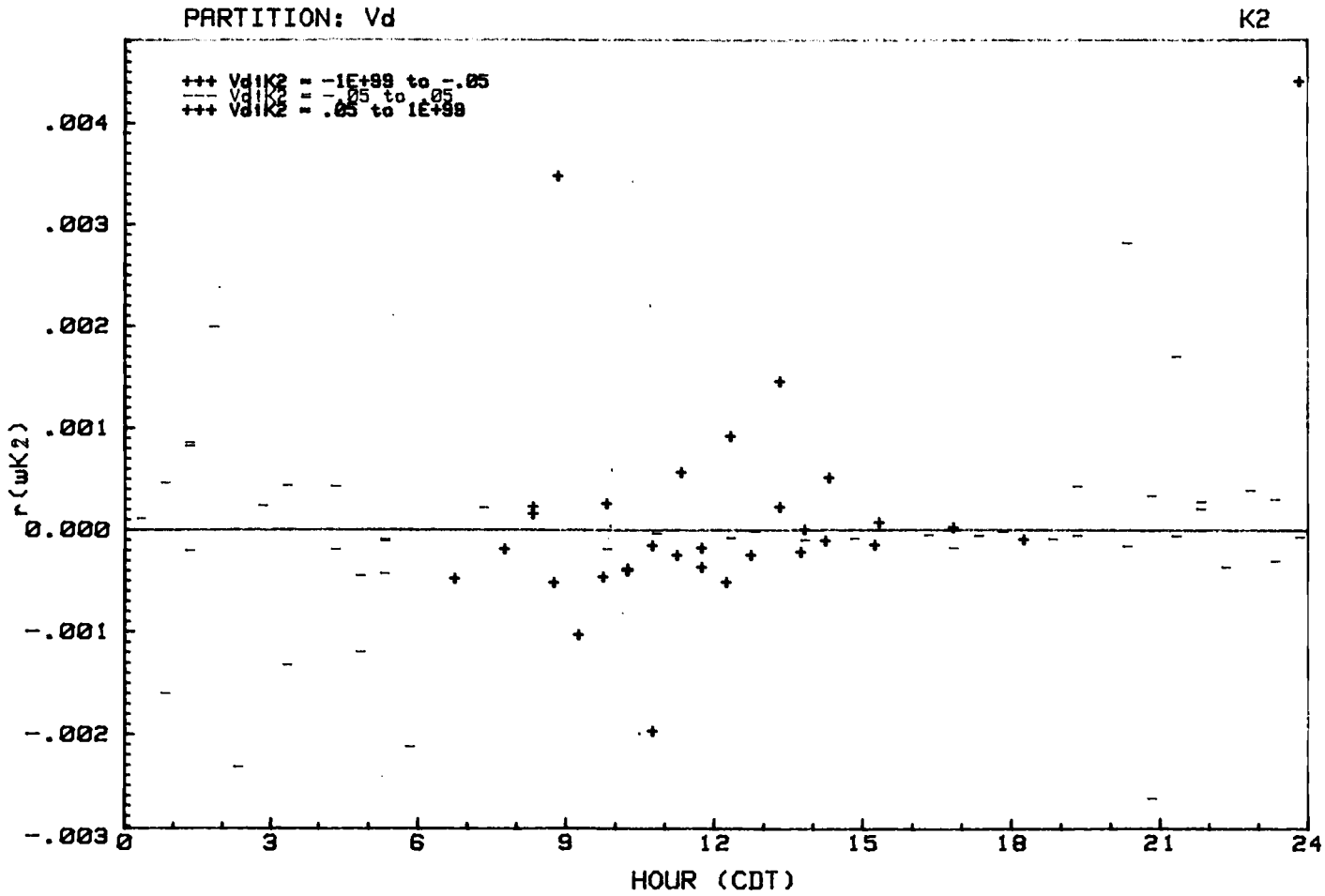

Figure 5.4b: Diurnal composite of w vs. particle count correlation coefficient (K2), partitioned by analog deposition velocity estimate.

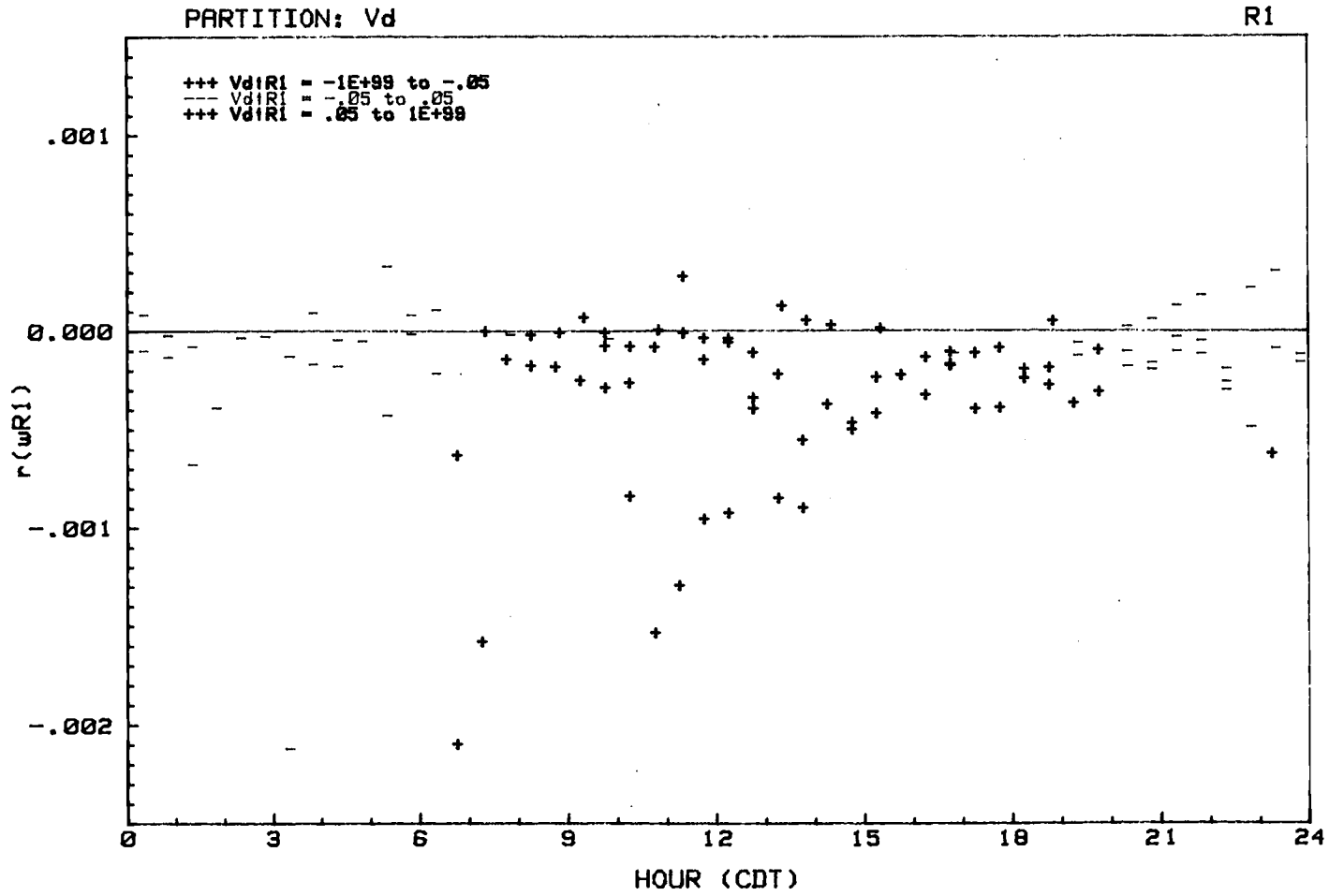

Figure 5.4c: Diurnal composite of w vs. particle count correlation coefficient (R1), partitioned by analog deposition velocity estimate.

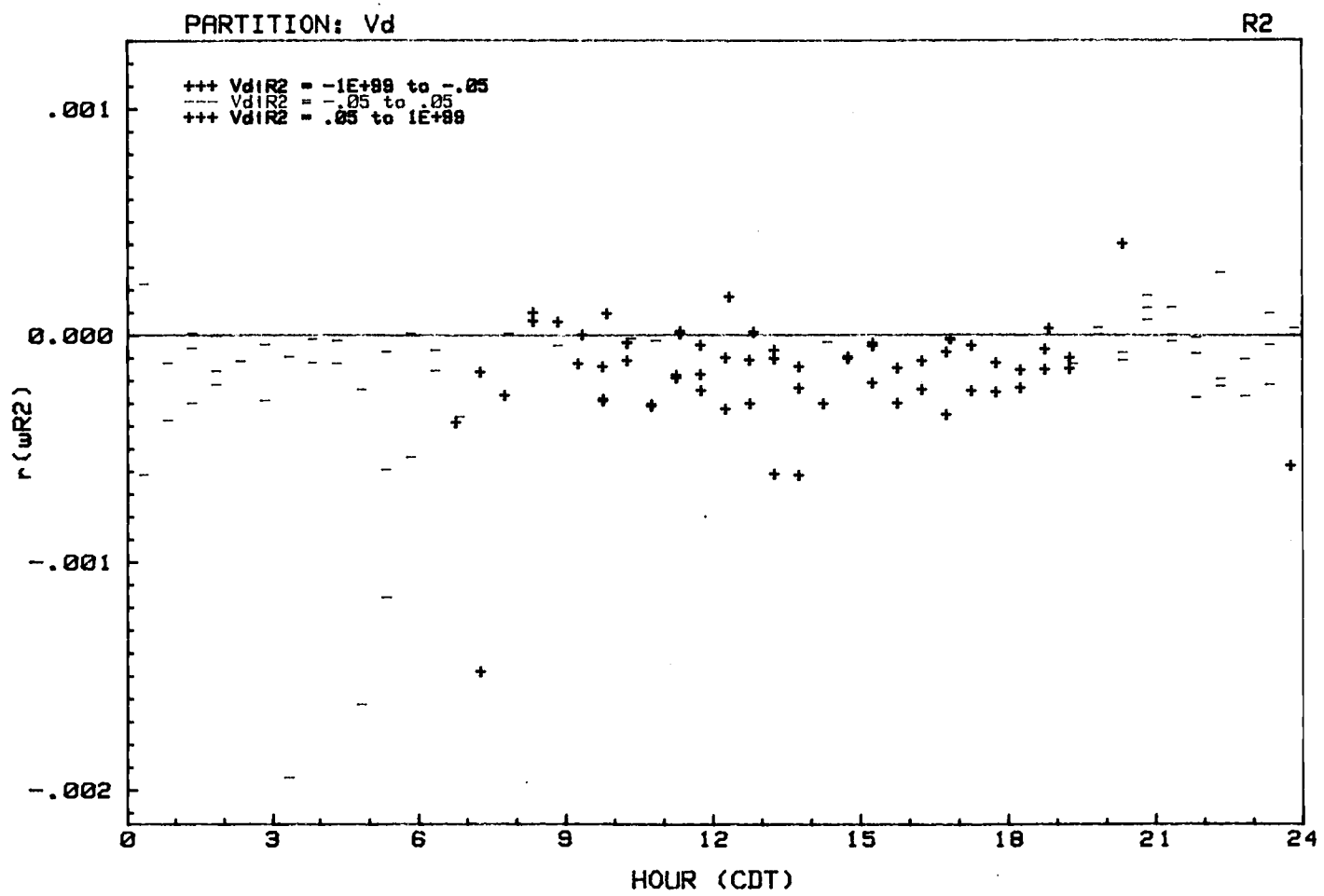

Figure 5.4d: Diurnal composite of w vs. particle count correlation coefficient (R2), partitioned by analog deposition velocity estimate.

variances described in Section (4), correlation coefficients for all valid blocks were calculated and are presented in Figures 5.4a-d. From this it is seen that the case study block was indeed quite representative, since the majority of the magnitudes fall below 0.0015. As this is below the 5% significance level, the only conclusion that may be drawn is that the flux process is too weak to be resolved in the presence of the given noise level. However, the distance between the majority of values and the 5% significance level is of interest, particularly since it is relatively larger than the distances between the deposition velocities and their 5% significance level ($1.96*SE(V_d)$).

In terms of future use of this type of sensor, the implications of this result are that either the noise level must be reduced through higher aspiration rates (and thereby higher count rates) or a stronger signal must be observed. The latter is an artificial constraint on the site and ambient conditions suitable for these measurements and may not be satisfied in the majority of interesting cases.

5.2 High relative humidity cases

One aspect of this data set which deserves examination is relative humidity effects on measured and actual particle fluxes. These effects may have significant magnitudes with respect to the current results. These results do not represent conclusive evidence but suggest mechanisms which deserve more careful attention in subsequent field studies. Theoretical and observational studies are reviewed; then results from the current field study are presented; finally, the

observations will be examined in light of the hypothesized effects and possible other confounding effects.

Two moisture effects discussed in the dry deposition literature are pertinent to the estimation of particle fluxes through the atmospheric surface layer. One is the actual change in the deposition velocity due to the increase in particle size by hygroscopicity or deliquescence that results from an increase in the ambient relative humidity. Theoretical predictions of this effect are given by Slinn & Slinn (1980) for deposition to natural water surfaces. $(NH_4)_2SO_4$ particles of radii 0.01-.05 μm were expected to experience deposition velocities reduced by a factor of two when exposed to relative humidities of 99-100% whereas 0.5-5 μm particle deposition velocities were thought to increase by one to two orders of magnitude under the same conditions.

The second effect is an apparent, but false, upward flux of particles (Sievering et al., 1982) illustrated by the schematic of Figure 5.5. The effect is in part due to the restriction of particle concentration measurements to a narrow range of radii which is located in a negative slope region of the particle size spectrum (where concentration increases with decreasing radius). The effect on a hygroscopic aerosol of increasing the ambient relative humidity is to shift its size distribution to the right (to larger radii). Through the narrow 'window', this shift is manifest as an increase in ambient concentration. When turbulent mixing of unsaturated air occurs over a moist surface, a vertical profile of horizontally averaged relative humidity results in which near-surface values approach 100%. It is conceivable, then, that the size distributions in turbulent eddys of

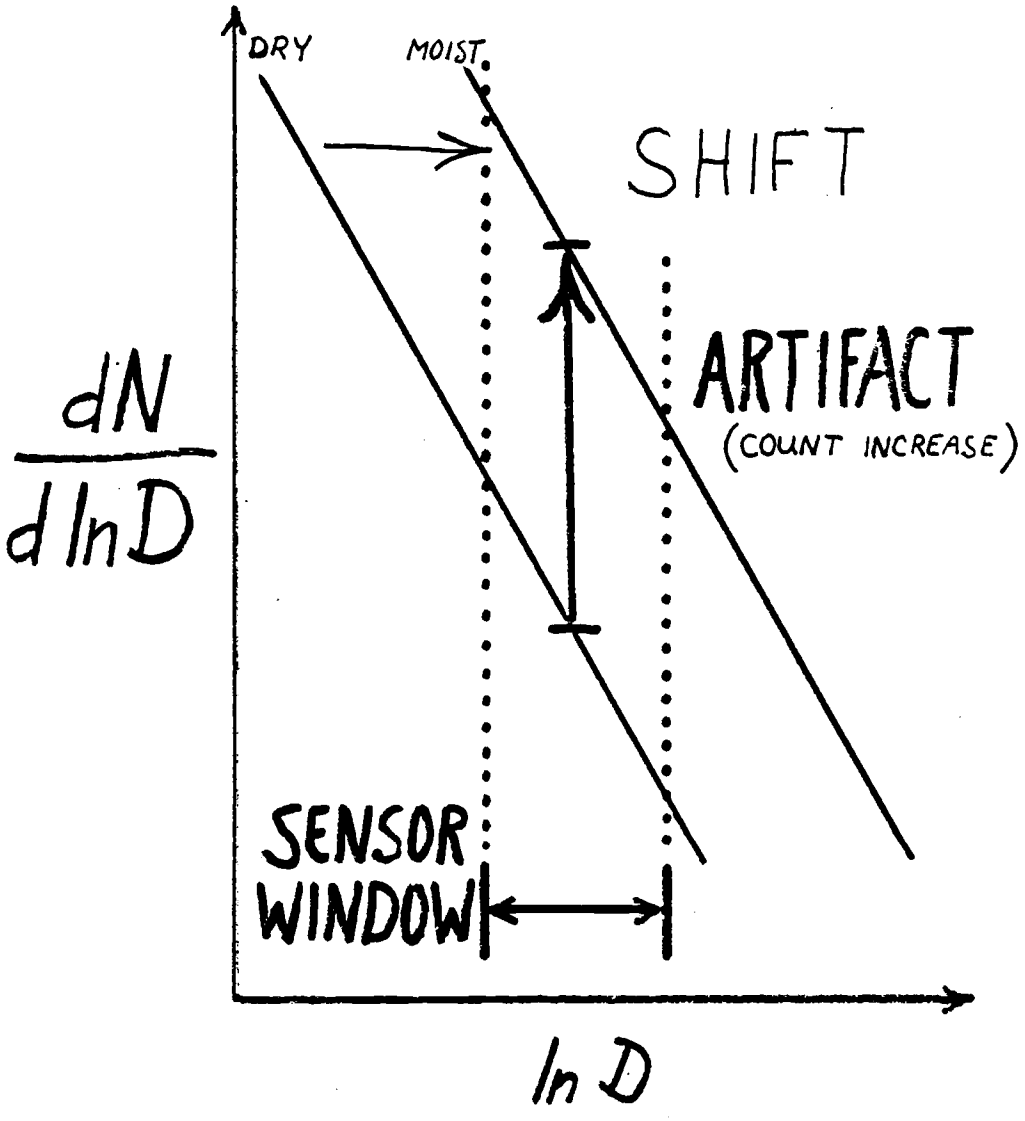

Figure 5.5:
Schematic diagram of cause of humidity gradient artifact particle flux. Background graph is idealized particle size distribution.

the aerosol shift back and forth as they become mixed with the drier(moister) air at the top(bottom) of the surface layer. Thus, the same correlation which is associated with upward vapor flux under such conditions could be responsible for the observance of higher particle counts in upward moving eddys and lower particle counts in downward moving eddys. The positive covariance, an artifact of the relative humidity gradient and the narrow size "window" of the sensor, could be mistaken for a particle source at the surface.

One piece of evidence that relative humidity may have been an important effect during this experiment, is a partitioning of the R1 and R2 deposition velocities according to ranges of relative humidity. Diurnal composites are presented in Figures 5.6a-b. Even though most of the daytime R1 and R2 deposition velocities are negative, the high humidity cases (+) seem to be slightly stronger negative than the low humidity cases (-). As indicated by Figure 5.7, the R1 and R2 size ranges include 0.30 to 2.5 μm which is a negative-slope portion of the size distribution.

The second piece of evidence to be considered here is an apparent diurnal cycle in particle concentration. Figure 5.8a-b are diurnal composites of particle count rate in which the time series have been maintained. The high correlation with the diurnal cycle in relative humidity (recall Figure 3.2) is evident suggesting that on time scales which represent equilibrium particle sizes, the particle size distribution responds to the relative humidity.

That there is a causal relationship between these two variables cannot be unequivocally shown from this data. Mechanisms other than the diurnal cycle in relative humidity may be responsible for the

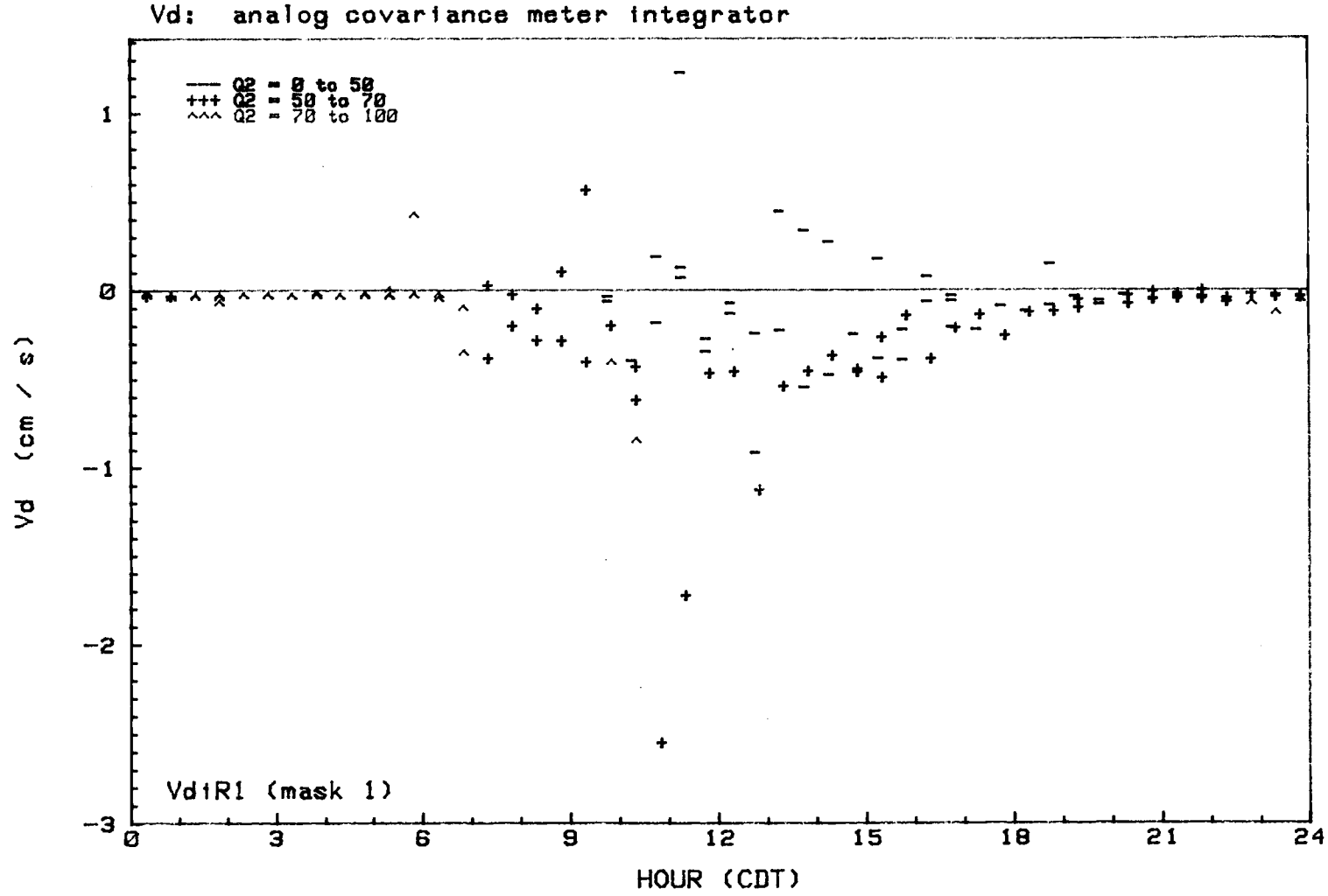

Figure 5.6a: Diurnal composite of deposition velocity (analog estimate, R1).

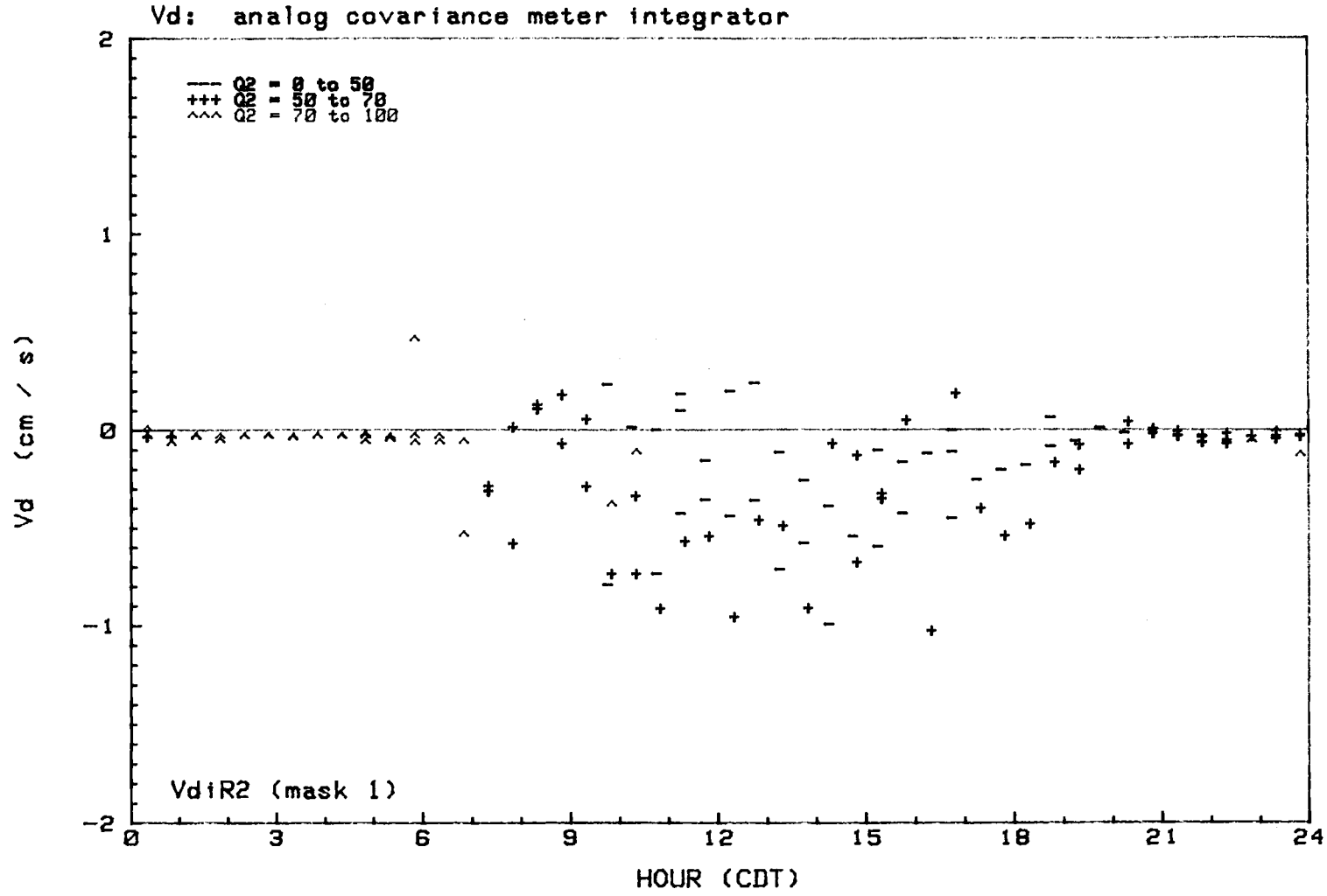

Figure 5.6b: Diurnal composite of deposition velocity (analog estimate, R2).

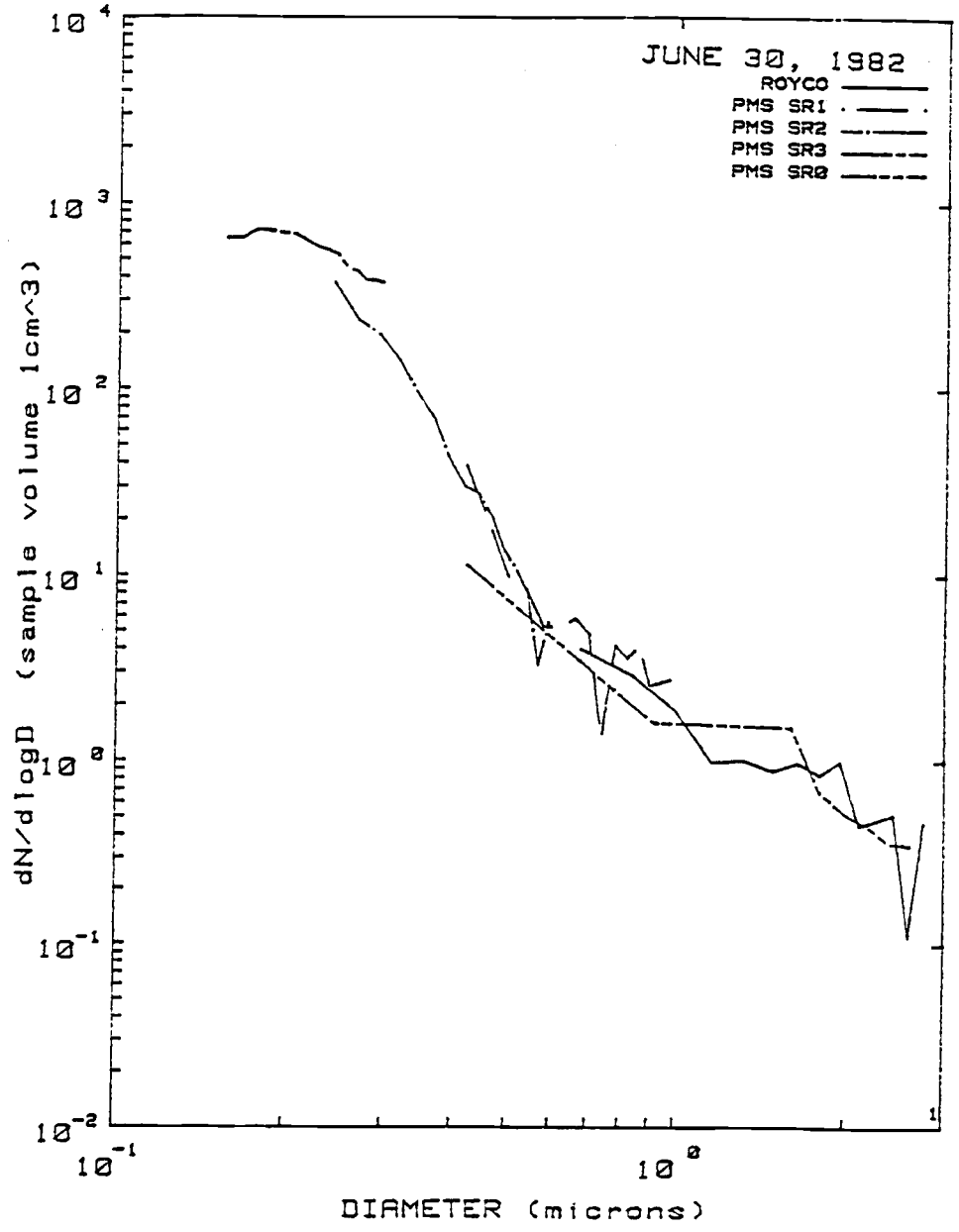

Figure5.7: Particle size distribution as measured by the ASAS-300A and Royco sensors on June 30.

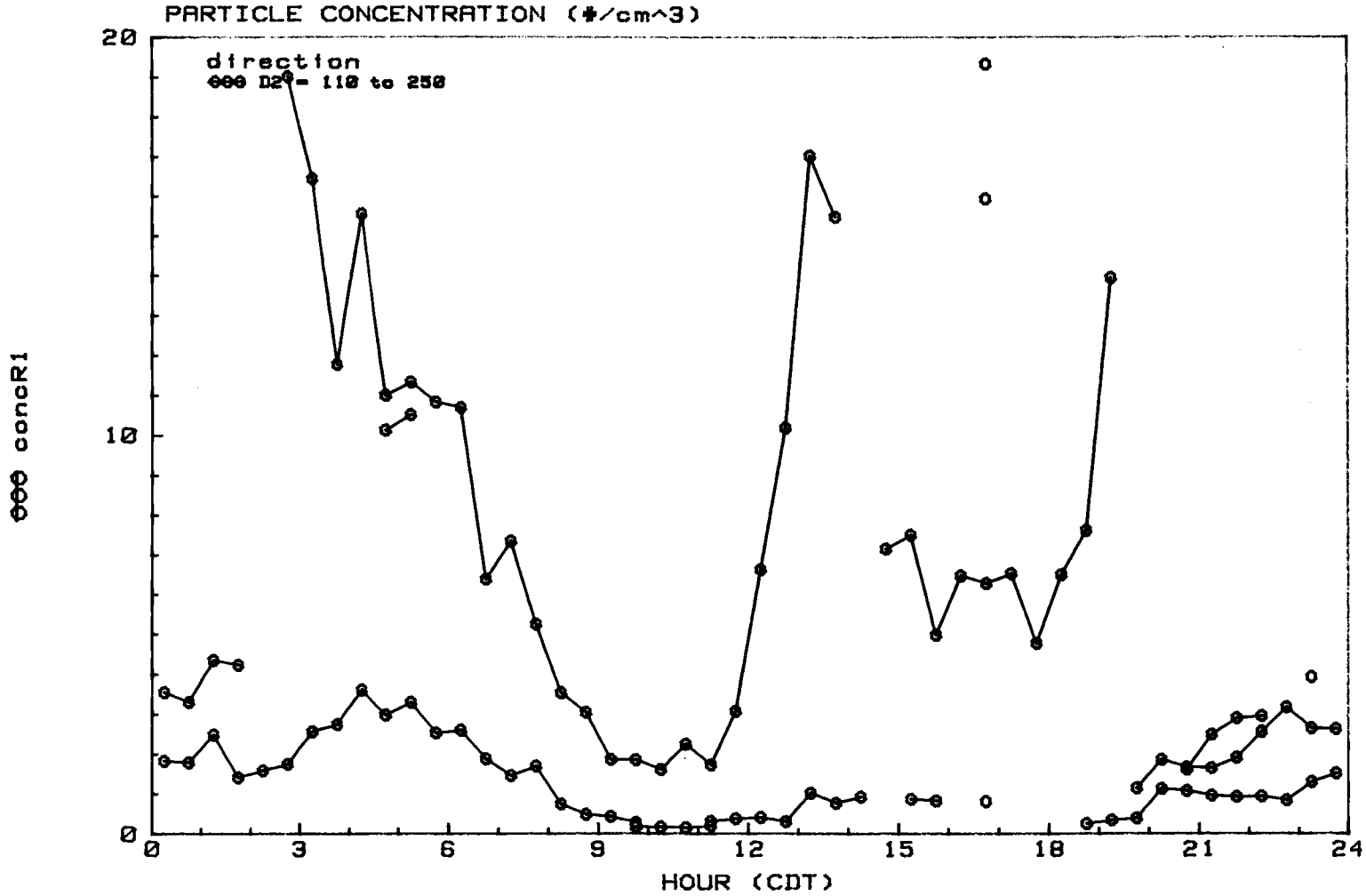

Figure 5.8a: Diurnal composite of particle cont rate (R1) with time series retained to illustrate diurnal cycle similar to that of relative humidity.

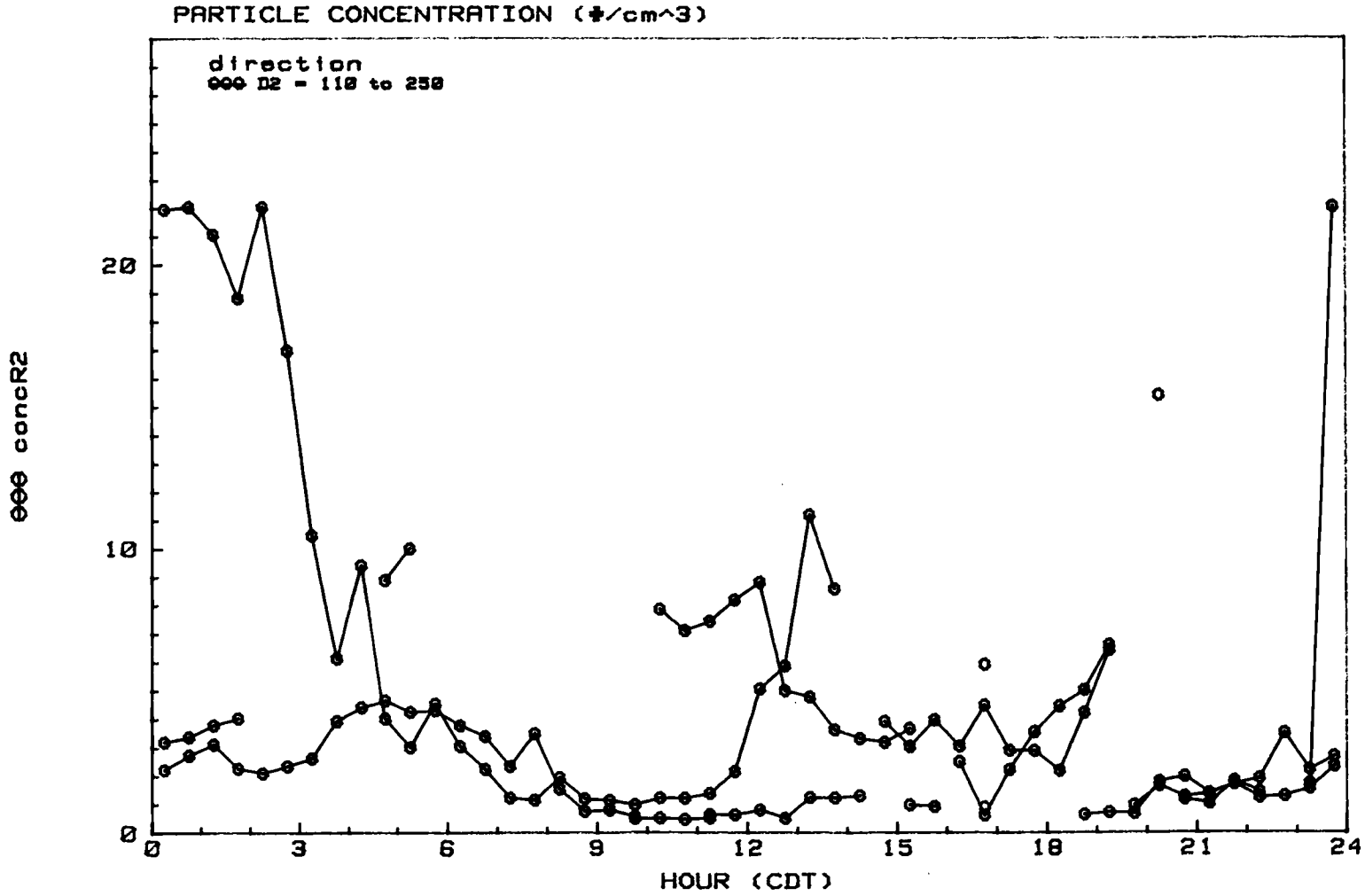

Figure 5.8b: Diurnal composite of particle count rate (R2) with time series retained to illustrate diurnal cycle similar to that of relative humidity.

observed correlation. It is possible that the diurnal cycle in particle concentration results from the diurnal cycle in the mixed layer height as it affects the initial dispersion in the aerosol source region. For example, pollutants from the St.Louis area may be dispersing into a shallower mixed layer at night. Measured concentrations at the site would reflect this cycle of transport time were short enough that phase lag would be minimal.

As was indicated in Section 1, the correction to the deposition velocity for diffusiophoresis effects has not been made in this work. The essential reason for this is that the marginal significance of the deposition velocities over their standard errors as shown in this and the previous sections cannot be corrected by this consideration.

6. CONCLUSIONS

In this section the experimental results will be summarized and the implications of these results to the objective of the thesis will be reviewed.

The discussion of data analysis is a reminder that care must be taken in the choice of a cutoff frequency for high pass filtering of turbulence data. Deposition velocities were presented which displayed considerable scatter about zero, particularly for the K1 and K2 size ranges. Magnitudes were generally less than 0.5 cm s^{-1} for K1 and K2 and less than 1 cm s^{-1} for R1 and R2. These estimates were shown to be marginally significant in terms of a simple standard error formulation. That is, the counting statistics of the particle sensors were shown to contribute enough random variability to the covariance to account for the majority of the variance in v_d. This result indicates that the measurements made in this experiment may not be used to make definitive estimates of the deposition velocity.

The fact that the K1 and K2 estimates of v_d are indeed marginally significant at the 5% level is interesting in view of the practically symmetric variance about zero. The suggestion here is either that the SE formulation is a slight underestimate or that the real particle flux actually exhibited some variation in sign. The former is more likely in view of the strict assumptions made in the derivation and in view of the correlation coefficient discussion, as will be reiterated below.

While precise estimates of v_d cannot be determined from this data set, the standard error that was presented may be viewed as a

nominal upper bound on the magnitude of the deposition velocity for these experimental conditions. This, in itself, is a significant contribution to the current body of knowledge since the appropriate order of magnitude remains controversial. This data set favors a value of about 0.1 cm sec^{-1}.

Perhaps the most important result of this work is the determination that higher resolution in particle concentration (higher count rates) will be required to resolve deposition velocities as small as 0.1 cm/s with acceptable precision. The recommendation made here of a 100-fold increase is based on the simple standard error formulation, which is not thought to be an overestimate, and is intended to resolve v_d to within 10%.

The examination of the correlation coefficient between vertical wind and particle count yielded several interesting results. Through the use of momentum flux contamination, the partitioning of the particle signal variance into a micrometeorological part and a Poisson counting part was shown to be valid and to produce a meaningful correlation coefficient. Viewing the Poisson variance as noise in a signal to noise ratio problem, it was demonstrated that the momentum flux was easily a strong enough signal to be determined through the current noise level but that the deposition velocity was not. From this point of view, it is apparent that a smaller ratio of σ_p^2 to σ_c^2 will be required to resolve the deposition velocity. If this smaller ratio is achieved, however, the assumptions on which the variance partitioning and standard error formulations are based will be less well satisfied; so these quantities will need to be rederived.

In comparing the standard error results with the correlation coefficient results the deposition velocity "signal" appears weaker in terms of the latter. One consideration which must be recalled is that the correlation coefficient is very sensitive to the correction of raw variances for data aquisition system attenuation. If the method chosen is only slightly biased then this disparity could be accounted for.

The discussion of relative humidity effects in Section 5 underlined the importance of their consideration in experimental design. Operation of duplicate sensors with inlet drying on one would be expected to address the question of possible artifact up-flux. However, a more sophisticated experiment would be required to document the real effect on deposition velocity of particle growth in the surface layer.

REFERENCES

Brook, R.R., 1978: The influence of water vapor fluctuations on turbulent fluxes, Boundary-Layer Meteorology, 15, pp 481-471.

DeGroot, M.H., 1975: Probability and Statistics, Addison-Wesley, Reading, Massachusetts.

Goldsmith, P. and F.G. May, 1966: Diffusiophoresis and Thermophoresis in Water Vapor Systems, In: Aerosol Science (Edited by C.N. Davies), Academic Press, New York.

Haight, F.A. 1967: Handbook of the Poisson Distribution, John Wiley & Sons, Inc., New York, N.Y.

Hicks, B.B., 1970: The measurement of atmospheric fluxes near the surface: a generalized approach, Journal of Applied Meteorology, 9, pp 386-388.

Hicks, B.B., 1972: Propellor anemometers as sensors of atmospheric turbulence, Boundary-Layer Meteorology, 3, pp 214-228.

Hicks, B.B. and M.L. Wesely, 1981: Heat and momentum transfer characteristics of adjacent fields of soybeans and maize, Boundary-Layer Meteorology, 20, pp 175-185.

Hicks, B.B., M.L. Wesely and J.L. Durham, 1980: Critique of Methods to Measure Dry Deposition: Workshop Summary, Environmental Protection Agency, Report No. EPA-600/9-80-050, October.

Hosker, R.P. and S.E. Lindberg, 1982: Review: Atmospheric deposition and plant assimilation of gases and particles, Atmospheric Environment, 16, pp 889-910.

Kaimal, J.C., 1975: Sensors and techniques for direct measurement of turbulent fluxes and profiles in the atmospheric surface layer, Atmospheric Technology, published NCAR, Boulder Colorado, 7, pp 7-14.

Kaimal, J.C., 1978: NOAA Instrumentation at the Boulder Atmospheric Observatory, in the Proceedings of the Fourth Symposium on Meteorological Observations and Instrumentation, American Meteorological Society, Denver, Colorado, April 10-14.

Kaimal,J.C., J.C. Wynqaard, Y. Isumi, and O.R. Cote, 1972: Spectral characteristics of surface-layer turbulence, Quarterly Journal of the Royal Meteorological Society, 98, pp 563-589.

Katen, P.C. and J.M. Hubbe, 1984: An evaluation of optical particle counter measurements of the dry deposition of atmospheric aerosol particles, submitted to Journal of Geophysical Research.

Mood, A.M., F.A. Graybill, and D.C. Boes, 1963: Introduction to the Theory of Statistics, 443 pp., McGraw-Hill Book Co.

Neumann, H.H., and G. den Hartog, 1984: Eddy correlation measurements of atmospheric fluxes of ozone, sulphur, and particulates during the Champaign intercomparison study, submitted to Journal of Geophysical Research.

Sehmel, G.A., 1973: Particle eddy diffusivities and deposition velocities for isothermal flow and smooth surfaces, Aerosol Science, 4, pp 125-138.

Sehmel, G.A., 1980: Particle and Gas Dry Deposition: a review, Atmospheric Environment, 14, pp 983-1011.

Sievering, H., 1982: Profile measurements of particle dry deposition velocity at an air/land interface, Atmospheric Environment, 16, pp 301-306.

Sievering, H., J. Eastman and J.A. Schmidt, 1982: Air-sea particle exchange at a NCAR shore oceanic site, Journal of Geophysical Research, 87, pp 11027-11037.

Sievering, H., 1983: Eddy flux and profile measurements of small-particle dry-deposition velocity at the Boulder Atmospheric Observatory (BAO), Proceedings of the Fourth International Conference on Precipitation Scavenging, Dry Deposition, and Resuspension, Pruppacher et al. Editors, Elsevier Science Publishing Co., Inc., New York, N.Y.

Slinn, W.G.N., P.C. Katen, M.A. Wolf, W.D. Loveland, L.F. Radke, E.L. Miller, L.J. Ghannam, B.W. Reynolds and D. Vickers, "Wet and dry deposition and resuspension of AFCT/TFCT fuel processing radionuclides, Final Report, SR-0980-10, September 1979, Air Resources Center, Oregon State University, Corvallis, Oregon, Available from NTIS, Springfield, Virginia.

Slinn, S.A. and W.G.N. Slinn, 1980: Predictions for particle deposition on natural waters, Atmospheric Environment, 14, pp 1013-1016.

Slinn, W.G.N., 1982: Predictions for particle deposition to canopies, Atmospheric Environment, 16, pp 1785-1794.

Slinn, W.G.N., 1983: A pot pourri of deposition and resuspension questions, Proceedings of the Fourth International Conference on Precipitation Scavenging, Dry Deposition, and Resuspension, H.R. Pruppacher, R.G. Semonin and W.G.N. Slinn, eds., Elsevier Science Publishing Co., New York.

Smith, S.D. and E.P. Jones, 1979: Dry-air boundary conditions for correction of eddy flux measurements, Boundary-Layer Meteorology, 17, pp 375-379.

Waldmann, L. and K.H. Schmitt, 1966: Thermophoresis and diffusiophoresis of aerosols, In: Aerosol Science (Edited by C.N. Davies), Academic Press, New York.

Webb, E.K., G.I. Pearman and R. Lenning, 1980: Correction of flux measurements for density effects due to heat and water vapor transfer, Quarterly Journal of the Royal Meteorological Society, 106, pp 85-100.

Wesely, M.L., B.B. Hicks, W.P. Dannevik, S. Frisella and R.B. Husar, 1977: An eddy-correlation measurement of particulate deposition from the atmosphere, Atmospheric Environment, 11, pp 561-563.

Wesely, M.L. and B.B. Hicks, 1979: Dry deposition and emission of small particles at the surface of the earth, Fourth Symposium on Turbulence, Diffusion and Air Pollution, American Meteorological Society, Boston, Mass., pp 510-513.

Wesely, M.L., D.R. Cook and R.M. Williams, 1981: Field measurements of small ozone fluxes to snow, wet bare soil and lake water, Boundary-Layer Meteorology, 20, pp 459-471.

Wesely, M.L., J.A. Eastman, D.H. Stedman and E.D. Yalvac, 1982: An eddy-correlation measurement of NO_2 flux to vegetation and comparison to O_3 flux, Atmospheric Environment, 16, pp 815-820.

Wesely, M.L., D.R. Cook and R.L. Hart, 1983: Fluxes of gases and particles above a deciduous forest in wintertime, Boundary-Layer Meteorology, 27, pp 237-255.